

## COSMIC-RAY CURRENT-DRIVEN TURBULENCE AND MEAN-FIELD DYNAMO EFFECT

IGOR ROGACHEVSKII<sup>1,2</sup>, NATHAN KLEEORIN<sup>1,2</sup>, AXEL BRANDENBURG<sup>2,3</sup>, AND DAVID EICHLER<sup>4</sup>

<sup>1</sup> Department of Mechanical Engineering, Ben-Gurion University of the Negev, POB 653, Beer-Sheva 84105, Israel

<sup>2</sup> NORDITA, Royal Institute of Technology and Stockholm University, Roslagstullsbacken 23, SE-10691 Stockholm, Sweden

<sup>3</sup> Department of Astronomy, AlbaNova University Center, Stockholm University, SE 10691 Stockholm, Sweden

<sup>4</sup> Department of Physics, Ben-Gurion University of the Negev, POB 653, Beer-Sheva 84105, Israel

Received 2012 March 21; accepted 2012 April 25; published 2012 June 7

### ABSTRACT

We show that an  $\alpha$  effect is driven by the cosmic-ray (CR) Bell instability exciting left–right asymmetric turbulence. Alfvén waves of a preferred polarization have maximally helical motion, because the transverse motion of each mode is parallel to its curl. We show how large-scale Alfvén modes, when rendered unstable by CR streaming, can create new net flux over any finite region, in the direction of the original large-scale field. We perform direct numerical simulations (DNSs) of a magnetohydrodynamic fluid with a forced CR current and use the test-field method to determine the  $\alpha$  effect and the turbulent magnetic diffusivity. As follows from DNS, the dynamics of the instability has the following stages: (1) in the early stage, the small-scale Bell instability that results in the production of small-scale turbulence is excited; (2) in the intermediate stage, there is formation of larger-scale magnetic structures; (3) finally, quasi-stationary large-scale turbulence is formed at a growth rate that is comparable to that expected from the dynamo instability, but its amplitude over much longer timescales remains unclear. The results of DNS are in good agreement with the theoretical estimates. It is suggested that this dynamo is what gives weakly magnetized relativistic shocks such as those from gamma-ray bursts (GRBs) a macroscopic correlation length. It may also be important for large-scale magnetic field amplification associated with CR production and diffusive shock acceleration in supernova remnants (SNRs) and blast waves from GRBs. Magnetic field amplification by Bell turbulence in SNRs is found to be significant, but it is limited owing to the finite time available to the super-Alfvénically expanding remnant. The effectiveness of the mechanisms is shown to be dependent on the shock velocity. Limits on magnetic field growth in longer-lived systems, such as the Galaxy and unconfined intergalactic CRs, are also discussed.

*Key words:* cosmic rays – instabilities – magnetic fields – turbulence

*Online-only material:* color figures

### 1. INTRODUCTION

Astrophysical blast waves are strongly suspected of amplifying the ambient magnetic field into which they propagate. Supernova remnants (SNRs), given detailed models for their ultra-high-energy gamma-ray emission, indicate magnetic fields that are considerably stronger than the several  $\mu\text{G}$  fields that are present in the interstellar medium. The exact strength of SNR magnetic fields depends on how small-scale bright spots are interpreted (Pohl 2009).

Gamma-ray burst (GRB) afterglows, which are attributed to relativistic blast waves, are generally best fit with a magnetic field strength that is much higher than interstellar magnetic fields. It has been suggested that the Weibel instability is responsible for the magnetic field production/amplification (Medvedev & Loeb 1999), but several difficulties with this proposal (Blandford & Eichler 1987) remain unsolved. First, the fastest growing Weibel-unstable modes are of very small scale, the ion plasma skin depth, and they should decay away resistively over the hydrodynamical timescale of the blast wave. Second, the electrons in the actual interstellar medium are already magnetized as they enter the shock, and they should therefore freeze the magnetic flux. The Weibel instability, which creates new flux, should therefore be suppressed at finite amplitudes, despite being unstable at infinitesimal amplitudes. It is not clear that these problems are resolved by simulations, which cannot be run over hydrodynamical timescales, and which do not always include initial electron magnetization. In this regard, the Bell instability (Bell 2004), which treats the thermal

plasma as a magnetized fluid, may be more relevant than kinetic approaches that ignore the electron magnetization, i.e., their gyroradii are small compared with the relevant length scales of the system.

Cosmic-ray (CR) protons above 200 TeV and iron nuclei above 3 PeV are difficult to account for with standard SNR parameters (Lagage & Cesarsky 1983), and magnetic field amplification would solve this problem if it occurs on a large scale. The smaller the scale of field amplification, the lower the maximum energy of the CRs that can be accelerated by the shock (Eichler & Pohl 2011).

Simulations of magnetic fields in the presence of CRs (Lucek & Bell 2000; Bell 2004) show magnetic field stretching. This is accompanied by a jumbling of the field lines into a more complicated geometry and a smaller coherence length. It has remained unclear whether this is merely turbulent field line stretching or there is an additional mechanism.

It has recently been noted by Bykov et al. (2011) that a circularly polarized Alfvén wave gives a net electromotive force (EMF) along the direction of the original magnetic field. Because CR protons preferentially excite Alfvén waves of a particular circular polarization, they generate a net EMF along the original magnetic field. The field growth is given by the curl of this EMF, which, for a plane wave, is  $\mathbf{k} \times \mathbf{B}$ , yielding a growing Alfvén mode, whose polarization vector  $\mathbf{k} \times \mathbf{B}$  is perpendicular to the original magnetic field. To lowest order, this does not amplify the field but merely bends it, and the question still remains as to whether (1) the field lines are merely getting stretched on this large scale, which would leave the net

flux through any large-scale surface unchanged, or (2) there is organized amplification, whereby the flux of magnetic field lines through a given large-scale surface is increased.

In this paper we note that the situation can result in an  $\alpha^2$  dynamo, in which a large-scale magnetic field can grow along its original direction and thus get amplified. The effect results from a nonlinear coupling between the individual waves that were demonstrated by Bykov et al. (2011) to grow. However, there is a maximum size over which such amplification can be effective. As the quantity  $\alpha$  has dimensions of velocity (in contrast to the stretching timescale, which has dimensions of time and which can be as short as the eddy turnover time of the turbulence), this maximum spatial scale is of the order of  $\alpha T$ , where  $T$  is the age of the blast wave. The magnetic field on this scale can grow by at most of the order of one  $e$ -fold over this time. On the other hand, because the field is amplified along its original direction, scales below the maximum scale can grow exponentially, in contrast to mere stretching, which would continually alter the scale as the field lines lengthen.

The formal objective of the present work is to show that the parameter  $\alpha$ , as defined in standard dynamo theory, is non-zero in the presence of CR streaming instabilities and to estimate its value. This will imply a maximum amount of growth on any given scale over any given time interval.

The partial pressure  $P^{\text{cr}} = n^{\text{cr}} \Gamma m_i c^2 / 3$  in CRs in any logarithmic interval of energy above energy  $E_{\text{min}}$  is about  $P^{\text{cr}} \sim \rho u_s^2 / \ln(E_{\text{max}}/E_{\text{min}}) \lesssim \rho u_s^2 / 10$  (Ellison & Eichler 1985). Here,  $u_s$  is the streaming velocity,  $\rho = n_i m_i$  is the plasma density,  $n_i$  is the interstellar number density of protons,  $m_i$  is the mass of a plasma ion,  $c$  is the speed of light, and  $\Gamma$  is the CR's Lorentz factor. Thus, the high-energy CR number density is

$$n^{\text{cr}} = \frac{3P^{\text{cr}}}{\Gamma m_i c^2} \sim \frac{3\rho u_s^2}{\Gamma m_i c^2 \ln(E_{\text{max}}/E_{\text{min}})}.$$

The CR current  $\mathbf{J}^{\text{cr}} = n^{\text{cr}} e \mathbf{u}_s$  due to CRs within a given logarithmic interval of CR energy can then be factored into dimensionless parameters as follows:

$$\mathcal{J} \equiv \frac{4\pi}{c} \frac{J^{\text{cr}}}{kB} = \frac{3}{2} \frac{u_s}{c} \frac{P^{\text{cr}}}{B^2/8\pi} \frac{eB}{k\Gamma m_i c^2}. \quad (1)$$

We will show in the present study that  $\mathcal{J}$  is a key parameter that determines large-scale magnetic field amplification. The last factor  $eB/(k\Gamma m_i c^2)$  in Equation (1) is the deflection of the CR over its passage through one scale length,  $k^{-1}$ , of the magnetic field. The derivation of the Bell instability that is caused by the CR current in plasma assumes that the deflection of the CR is small. For the firehose instability, the subject of a separate investigation, it can be larger than unity, as the CRs would be bound to the field lines. However, a situation can occur in which the CRs maintain a steady anisotropy,  $A$ , even if they scatter, and the choice for the streaming velocity is then  $u_s = A c$ , and the shock velocity is assumed to be approximately the same.

The factor  $u_s/c$  is typically of the order of  $10^{-2}$  or less, both for the Galaxy as a whole, where the anisotropy is limited by direct measurements, and for the CRs accelerated by forward shocks of blast waves from SNRs, where the CR precursor moves essentially at the shock velocity, typically  $10^{-3}$  to  $10^{-2}$  times  $c$ . Very young SNRs can have somewhat higher shock velocities, but the CR accelerated in them may then be more prone to adiabatic losses. Note that because we assume the streaming velocity to be the velocity of the shock, we may

allow for the possibility that CRs scatter in our estimate of the CR current. But we still have to limit the time over which a given parcel of fluid is exposed to the CR current to be less than the shock crossing time—the time it takes the shock to cross the length of the CR precursor at that energy.

The factor  $3P^{\text{cr}}/(B^2/4\pi)$  is of the order of unity for the Galaxy as a whole if all relativistic CRs are included. In this case, the anisotropy must be taken to be at most  $10^{-3}$  and  $u_s \lesssim 10^{-3}c$ . In the case of supernova blast waves, the factor  $3P^{\text{cr}}/(B^2/4\pi)$  can be as high as  $\sim u_s^2/v_A^2$ , where  $v_A$  is the Alfvén speed. Thus, the CR pressure can be a significant fraction of the ram pressure  $\rho u_s^2$  (see, e.g., Ellison & Eichler 1985).

Altogether, we can choose a plausible value for  $\mathcal{J}$  of  $\sim 3u_s^3/cv_A^2 \ln(E_{\text{max}}/E_{\text{min}})$ , which can range from  $10^4$  for young SNRs ( $u_s \sim c/10 \sim 10^3 v_A$ ) to order unity for old ones. For the Galaxy as a whole, we are probably limited to  $3P^{\text{cr}}/(B^2/4\pi) \lesssim 1$ . For collisionless shock waves generated in the interstellar medium by GRBs, the value of  $\mathcal{J}$  can be enormous—of order  $10^{14}$ —and the  $\alpha$  effect may be particularly effective in that context. This will be discussed in greater detail below, where relativistic effects are included more carefully.

The physical time over which the mechanism can operate on a given patch of upstream fluid in the case of an SNR is one expansion time, or  $R_s/u_s$ , where  $R_s$  is the radius of the forward shock. As  $u_s$  does not appear explicitly in the simulation parameters, we use the above expression  $\mathcal{J} \sim u_s^3/cv_A^2$  to substitute for  $u_s$  in terms of  $J^{\text{cr}}$  and  $v_A$ . For the Galaxy as a whole, we are limited by the Hubble time to be about  $10^4 R_G/v_A$ , where  $R_G$  is the size of the Galaxy.

## 2. GOVERNING EQUATIONS

We consider magnetohydrodynamic (MHD) flows consisting of background plasma ions of number density  $n_i$ , electrons of number density  $n_e$ , and CR protons of number density  $n^{\text{cr}}$ . The equation of motion in MHD flows with CRs imbedded in a background plasma reads (Chen 2010)

$$\rho \frac{D\mathbf{U}}{Dt} = -\nabla P + \frac{1}{c} \mathbf{J} \times \mathbf{B} + e(n_i - n_e) \mathbf{E} + \mathbf{F}_v, \quad (2)$$

where  $D/Dt = \partial/\partial t + \mathbf{U} \cdot \nabla$  is the advective derivative;  $\mathbf{U}$  is the fluid velocity;  $\rho$  and  $P$  are the fluid density and pressure, respectively;  $\mathbf{E}$  and  $\mathbf{B}$  are the electric and magnetic fields; and  $\mathbf{F}_v$  is the viscous force. The densities of the plasma current,  $\mathbf{J}$ , and of CR protons,  $\mathbf{J}^{\text{cr}}$ , are the sources of magnetic field in Maxwell's equations:

$$\nabla \times \mathbf{B} = \frac{4\pi}{c} (\mathbf{J} + \mathbf{J}^{\text{cr}}), \quad (3)$$

$$\nabla \times \mathbf{E} = -\frac{1}{c} \frac{\partial \mathbf{B}}{\partial t}, \quad (4)$$

with Ohm's law:  $\mathbf{J} = \sigma(\mathbf{E} + c^{-1} \mathbf{U} \times \mathbf{B})$ , where  $\sigma$  is the electrical conductivity of the gas, and we have neglected in Equation (3) the displacement current, because the conductivity is high and the fluid motions are slow compared with the speed of light. These equations yield the induction equation,

$$\frac{\partial \mathbf{B}}{\partial t} = \nabla \times (\mathbf{U} \times \mathbf{B} - \eta \nabla \times \mathbf{B} + c \mathbf{J}^{\text{cr}}/\sigma), \quad (5)$$

where  $\eta = c^2/4\pi\sigma$  is the magnetic diffusivity. We assume quasi-neutrality for the whole system, i.e.,  $n_i + n^{\text{cr}} = n_e$ , and

Equation (2) reads

$$\rho \frac{D\mathbf{U}}{Dt} = -\nabla P + \frac{1}{4\pi}(\nabla \times \mathbf{B}) \times \mathbf{B} + \mathbf{F}_v - \frac{1}{c} \mathbf{J}^{\text{cr}} \times \mathbf{B} + \frac{1}{c} e n^{\text{cr}} (\mathbf{U} \times \mathbf{B}), \quad (6)$$

where we have used Equation (3) and assumed that  $|\mathbf{J}/\sigma| \ll c^{-1}|\mathbf{U} \times \mathbf{B}|$ , i.e., we consider plasma flows with large hydrodynamic and magnetic Reynolds numbers. Hereafter, we assume that the CR velocity is much larger than fluid velocity  $\mathbf{U}$ , so that the last term in Equation (6) vanishes. The plasma density is determined by the continuity equation:

$$\frac{\partial \rho}{\partial t} + \nabla \cdot \rho \mathbf{U} = 0. \quad (7)$$

Following Bell (2004), let us consider the equilibrium:  $\mathbf{J}^{\text{eq}} + \mathbf{J}^{\text{cr}} = 0$ ,  $\mathbf{B}^{\text{eq}} = \mathbf{B}_* = \text{const}$ ,  $\mathbf{U}^{\text{eq}} = 0$ , and  $\rho^{\text{eq}} = \rho_* = \text{const}$ . Linearized Equations (5)–(7) for small perturbations yield the following dispersion relation:

$$\gamma^2 (\gamma \gamma_B + \omega_s^2) (\gamma^2 + \omega_A^2) = \omega_A^2 \left( \gamma \gamma_B \frac{k^2}{k_z^2} + \omega_s^2 \right) \times \left[ \left( \frac{\omega^{\text{cr}} k_z}{k} \right)^2 - \omega_A^2 - \gamma^2 \right], \quad (8)$$

where  $\omega_A = \mathbf{k} \cdot \mathbf{v}_A$  is the frequency of the Alfvén waves,  $\omega_s = kc_s$  is the frequency of the sound waves,  $c_s$  is the sound speed,  $\mathbf{k}$  is the wavenumber,  $v_A = \mathbf{B}_*/(4\pi\rho)^{1/2}$  is the Alfvén speed,  $\omega^{\text{cr}} = c^{-1} J^{\text{cr}} (4\pi/\rho)^{1/2}$ ,  $\gamma = \gamma_B + \eta k^2$ ,  $\gamma_B$  is the growth rate of an instability, and we have considered the case where the equilibrium magnetic field  $\mathbf{B}_*$  and  $\mathbf{J}^{\text{cr}}$  are directed along the  $z$ -axis.

In this system, the non-resonant Bell instability (Bell 2004; Lucek & Bell 2000) is excited by the CR current that causes growing MHD modes. The growth rate of this instability for  $\beta \gg 1$  that follows from Equation (8) is given by

$$\gamma_B = \left[ \frac{|\omega_A \omega^{\text{cr}} k_z|}{k} - \omega_A^2 \right]^{1/2} - \eta k^2, \quad (9)$$

where  $\beta$  is the ratio of gas pressure to magnetic pressure. For incompressible MHD modes  $\tilde{\mathbf{b}}(\mathbf{k}) = i(\mathbf{k} \cdot \mathbf{B}_*) \tilde{\mathbf{u}}(\mathbf{k})/\gamma_B$  (Bell 2004), where  $\tilde{\mathbf{u}}$  and  $\tilde{\mathbf{b}}$  are perturbations of velocity and magnetic field.

When  $\beta \ll 1$ , the growth rate of this instability that follows from Equation (8) is given by

$$\gamma_B = \frac{|\omega_A|}{\sqrt{2}} \left\{ \left[ \left( 1 - \frac{k}{k_z} \right)^2 + \left( \frac{2\omega^{\text{cr}}}{\omega_A} \right)^2 \right]^{1/2} - \left( 1 + \frac{k^2}{k_z^2} \right) \right\} - \eta k^2. \quad (10)$$

The nonlinear stage of this instability has been investigated in a number of publications (see, e.g., Bell 2004, 2005; Pelletier 2006; Reville 2008; Zirakashvili et al. 2008; Amato & Blasi 2009; Luo & Melrose 2009; Vladimirov et al. 2009; Zweibel & Everett 2010; Bykov et al. 2011, 2012). These studies have demonstrated that this instability produces small-scale

turbulence with cascading of turbulence energy into larger and smaller scales.

In this paper, we discuss the possibility of mean-field dynamo action caused by the interaction of mean electric current of CR particles with small-scale background homogeneous turbulence produced by the Bell instability. This paper can be considered as an extension of the recent study by Bykov et al. (2011), who demonstrated, using a multi-scale quasi-linear mean-field approach, that small-scale Bell-type turbulence can result in the growth of long-wavelength obliquely propagating modes (Bykov et al. 2011).

### 3. LARGE-SCALE INSTABILITY

In this section, we discuss mean-field dynamo action in small-scale turbulence produced by the Bell instability in a plasma with a given mean electric current of CR ions. The importance of this effect is determined by the ratio of the CR current to the ambient field; see Equation (1).

#### 3.1. Mean-field Dynamo Equations

We use a mean-field approach in which magnetic and velocity fields are divided into mean and fluctuating parts,  $\mathbf{U} = \bar{\mathbf{U}} + \mathbf{u}$  and  $\mathbf{B} = \bar{\mathbf{B}} + \mathbf{b}$ , where  $\mathbf{u}$  and  $\mathbf{b}$  are fluctuations of velocity and magnetic field,  $\bar{\mathbf{B}}$  and  $\bar{\mathbf{U}}$  are the mean magnetic and velocity fields, and the fluctuating fields have zero mean values. We consider the case when magnetic and fluid Reynolds numbers are large. This implies that the nonlinear terms in the induction and Navier–Stokes equations are much larger than the dissipative and viscous terms. In this case the quasi-linear approach for determining the turbulent transport coefficients (e.g., the  $\alpha$  effect and turbulent magnetic diffusivity) does not work. We use instead the spectral  $\tau$  relaxation approximation (Orszag 1970; Pouquet et al. 1976; Kleeorin et al. 1990; Rogachevskii & Kleeorin 2004) that is valid for large magnetic and fluid Reynolds numbers. A justification for the  $\tau$  approximation in different situations has been performed in numerical simulations and analytical studies (see, e.g., Brandenburg & Subramanian 2005; Rogachevskii et al. 2011). For more details see Appendix A.3.

Averaging Equations (5) and (6) over an ensemble of turbulent eddies yields the following mean-field equations:

$$\frac{\partial \bar{\mathbf{B}}}{\partial t} = \nabla \times (\bar{\mathbf{U}} \times \bar{\mathbf{B}} + \overline{\mathbf{u} \times \mathbf{b}} - \eta \nabla \times \bar{\mathbf{B}}), \quad (11)$$

$$\bar{\rho} \frac{D\bar{\mathbf{U}}}{Dt} = -\nabla \bar{P} + \frac{1}{4\pi} (\nabla \times \bar{\mathbf{B}}) \times \bar{\mathbf{B}} - \frac{1}{c} \bar{\mathbf{J}}^{\text{cr}} \times \bar{\mathbf{B}} + \frac{1}{c} e n^{\text{cr}} (\bar{\mathbf{U}} \times \bar{\mathbf{B}}) - \nabla_j \overline{u u_j} + \bar{\mathbf{F}}_v, \quad (12)$$

where  $\mathcal{E}(\bar{\mathbf{B}}) = \overline{\mathbf{u} \times \mathbf{b}}$  is the mean EMF and  $\bar{\mathbf{J}}^{\text{cr}}$  is the mean density of the electric current of CR particles. For large hydrodynamic and magnetic Reynolds numbers we can neglect kinematic viscosity,  $\nu$ , and magnetic diffusivity,  $\eta$ , in comparison with the turbulent viscosity and turbulent magnetic diffusion.

#### 3.2. Contributions to the $\alpha$ Effect

We will show in this study that, formally, there are two contributions to the  $\alpha$  effect, caused by (1) existing *kinetic helicity* produced by the Bell instability (referred to as  $\mathbf{u}^{(0)} \cdot (\nabla \times \mathbf{u}^{(0)})$  below) and (2) correlations in the forcing by the mean CR current

in the presence of small-scale magnetic fluctuations that create further perturbation  $\mathbf{u}^{(1)}$  in the velocity field  $\mathbf{u}^{(0)}$ . Effect (2) causes opposite sides of a magnetic loop to be forced in opposite directions, thereby twisting the loop out of its original plane. The distinction between the two terms may be more formal than physical. That is, in an unstable circularly polarized Alfvén mode, the additional helicity added by the CR forcing term is merely a continuation of the process that formed the already existing helicity.

The  $\alpha$  effect, however, is distinct from the linear growth of the circularly polarized Alfvén wave. It can be thought of as one circularly polarized Alfvén wave riding on another, somewhat longer wavelength Alfvén wave (which need not be circularly polarized). The longer wave makes a perpendicular component to the original field, while the stretching of the perpendicular component (into a loop, say), together with the twisting of the loop, restores newly created flux back into the original direction. It is the *nonlinear coupling* of two waves, each of which is of the sort discussed by Bykov et al. (2011). This coupling can scatter energy in the two modes of wavenumbers  $k_1$  and  $k_2$  into modes of much longer wavelength and thereby amplify the field at large scale in its original direction.

Let us consider the case where the equilibrium uniform mean magnetic field  $\overline{\mathbf{B}}_*$  and the mean density of the electric current of accelerated particles  $\overline{\mathbf{J}}^{\text{cr}}$  are directed along the  $z$ -axis. We take into account effects that are linear in perturbations of the mean magnetic field:  $\tilde{\mathbf{B}} = \overline{\mathbf{B}} - \overline{\mathbf{B}}_*$ , i.e., we consider kinematic mean-field dynamo.

The first contribution to the  $\alpha$  effect is caused by the helical part of the turbulence. A non-zero kinetic helicity is caused by the Bell instability that results in the production of small-scale helical turbulence. This contribution to the mean EMF is given by  $\mathcal{E}_i^{(I)} = \alpha_{ij}^{(I)} \tilde{B}_j + \dots$  (see Appendix A.6), where  $\alpha_{ij}^{(I)} = \alpha_1^{\text{cr}} \delta_{ij}$  is an isotropic  $\alpha$  effect,

$$\alpha_1^{\text{cr}} = -C_1 \tau_0 \overline{\mathbf{u}^{(0)} \cdot (\nabla \times \mathbf{u}^{(0)})}, \quad (13)$$

with coefficient  $C_1 \approx 1/3$ , and dots referring to higher-order terms that will be considered later in Section 4.2. In the rest of this section the dots will not be noted explicitly. Here,  $\mathbf{u}^{(0)}$  are the velocity fluctuations of the background turbulence. Equation (13) is a well-known result for the  $\alpha$  effect caused by kinetic helicity of the turbulence (see Krause & Rädler 1980; Moffatt 1978; Parker 1979; Zeldovich et al. 1983).

The second contribution to the  $\alpha$  effect is caused by incompressible and non-helical parts of the turbulence interacting with the mean CR current. In particular, this contribution to the mean EMF is given by  $\mathcal{E}_i^{(II)} = \alpha_{ij}^{(II)} \tilde{B}_j$ , where  $\alpha_{ij}^{(II)} = \alpha_2^{\text{cr}} (\delta_{ij} + e_i e_j)$  (see Appendix A.6),

$$\alpha_2^{\text{cr}} = C_2 \left( \frac{4\pi \overline{\mathbf{J}}^{\text{cr}} \ell_0}{c \overline{B}_*} \right)^{1/2} \overline{V}_A \text{sgn}(\overline{\mathbf{J}}^{\text{cr}} \cdot \mathbf{B}_*), \quad (14)$$

$\overline{V}_A = \overline{B}_*/(4\pi\overline{\rho})^{1/2}$  is the mean Alfvén speed based on the equilibrium mean magnetic field  $\overline{\mathbf{B}}_*$ ,  $\mathbf{e}$  is the unit vector directed along  $\overline{\mathbf{B}}_*$ ,  $C_2 = 4(q-1)/3(2q-3)$ , and  $q$  is the exponent of the energy spectrum of the turbulence. Note that  $C_2 \approx 8/3$  for  $q = 5/3$ . The total  $\alpha$  effect is the sum of the two contributions:

$$\alpha_{ij}^{\text{cr}} = \alpha_{ij}^{(I)} + \alpha_{ij}^{(II)}. \quad (15)$$

The mechanism of the second contribution,  $\alpha_{ij}^{(II)}$ , to the  $\alpha$  effect can be understood by the following reasoning. Tangling of the mean magnetic field  $\tilde{\mathbf{B}} = \overline{\mathbf{B}} - \overline{\mathbf{B}}_*$  by velocity fluctuations of the background anisotropic turbulence  $\mathbf{u}^{(0)}$  produces magnetic fluctuations:

$$\frac{\partial \mathbf{b}^{(1)}}{\partial t} \propto (\tilde{\mathbf{B}} \cdot \nabla) \mathbf{u}^{(0)}. \quad (16)$$

The generated magnetic fluctuations  $\mathbf{b}^{(1)}$  interacting with the CR current  $\overline{\mathbf{J}}^{\text{cr}}$  produce additional velocity fluctuations:

$$\frac{\partial \mathbf{u}^{(1)}}{\partial t} \propto -\frac{1}{c\overline{\rho}} \overline{\mathbf{J}}^{\text{cr}} \times \mathbf{b}^{(1)}. \quad (17)$$

These velocity fluctuations contribute to the mean EMF  $\mathcal{E}^{(II)} = \overline{\mathbf{u}^{(1)} \times \mathbf{b}^{(0)}}$ . Here,  $\mathbf{b}^{(0)}$  are the magnetic fluctuations resulting directly from the Bell instability, just like the velocity perturbations  $\mathbf{u}^{(0)}$ . In particular, the stretching of the original magnetic field determined by Equation (16) and rotation of the stretched magnetic loop determined by Equation (17) create an electric field  $\mathcal{E}^{(II)}$  along the original magnetic field  $\tilde{\mathbf{B}}$ . The Lorentz force in Equation (17) plays the role of rotation of a magnetic loop. Using Equations (16) and (17), we can estimate the mean EMF  $\mathcal{E}^{(II)}$  using dimensional reasoning. Indeed, the velocity fluctuations can be estimated as

$$\mathbf{u}^{(1)} \propto -\frac{\tau}{c\overline{\rho}} \overline{\mathbf{J}}^{\text{cr}} \times \mathbf{b}^{(1)} \propto -\frac{\tau^2}{c\overline{\rho}} \overline{\mathbf{J}}^{\text{cr}} \times (\tilde{\mathbf{B}} \cdot \nabla) \mathbf{u}^{(0)}, \quad (18)$$

where  $\tau$  is the characteristic time of the turbulence. Therefore, the mean EMF  $\mathcal{E}^{(II)}$  is estimated as

$$\mathcal{E}_i^{(II)} \propto \frac{\tau^2}{c\overline{\rho}} (\overline{J_i^{\text{cr}} \overline{b_n^{(0)} \nabla_j u_n^{(0)}}} - \overline{J_n^{\text{cr}} \overline{b_n^{(0)} \nabla_j u_i^{(0)}}}) \tilde{B}_j. \quad (19)$$

The mean EMF  $\mathcal{E}^{(II)}$  is proportional to the mean magnetic field  $\tilde{\mathbf{B}}$ , i.e.,  $\mathcal{E}_i^{(II)} = a_{ij} \tilde{B}_j$  and the tensor  $a_{ij}^{(II)}$  is the symmetric part of  $a_{ij}$ . Therefore,

$$\alpha_{ij}^{(II)} \propto \frac{\tau^2}{2c\overline{\rho}} (\overline{J_i^{\text{cr}} \overline{b_n^{(0)} \nabla_j u_n^{(0)}}} + \overline{J_j^{\text{cr}} \overline{b_n^{(0)} \nabla_i u_n^{(0)}}}) - \overline{J_n^{\text{cr}} \overline{b_n^{(0)} \nabla_j u_i^{(0)}}} - \overline{J_n^{\text{cr}} \overline{b_n^{(0)} \nabla_i u_j^{(0)}}}). \quad (20)$$

Note that in many kinds of background turbulence, the tensor  $\overline{b_i^{(0)} u_j^{(0)}}$  and the background mean EMF  $\mathcal{E}^{(0)} = \mathbf{u}^{(0)} \times \mathbf{b}^{(0)}$  vanish. On the other hand, for the turbulence produced by the Bell instability, the tensor  $\overline{b_i^{(0)} u_j^{(0)}}$  does not vanish.

Now let us compare this mechanism for the  $\alpha$  effect with the standard mechanism based on nonzero kinetic helicity. The mean EMF  $\mathcal{E}^{(I)} = \overline{\mathbf{u}^{(0)} \times \mathbf{b}^{(1)}}$ , where the magnetic fluctuations  $\mathbf{b}^{(1)}$  are generated by the tangling of the mean magnetic field  $\tilde{\mathbf{B}}$  by the velocity fluctuations of the background turbulence  $\mathbf{u}^{(0)}$ . Therefore, the mean EMF is given by

$$\mathcal{E}^{(I)} \propto \overline{\mathbf{u}^{(0)} \times (\tilde{\mathbf{B}} \cdot \nabla) \mathbf{u}^{(0)}}, \quad (21)$$

and the  $\alpha_{ij}^{(I)}$  tensor is

$$\alpha_{ij}^{(I)} \propto \tau (\varepsilon_{imn} \overline{u_m^{(0)} \nabla_j u_n^{(0)}} + \varepsilon_{jnm} \overline{u_m^{(0)} \nabla_i u_n^{(0)}}), \quad (22)$$

where the kinetic helicity is produced by the Bell instability and  $\chi_{ij} = \varepsilon_{inm} \overline{u_m^{(0)} \nabla_j u_n^{(0)}} + \varepsilon_{jnm} \overline{u_m^{(0)} \nabla_i u_n^{(0)}}$  is the symmetric tensor of the kinetic helicity for anisotropic turbulence. Using the model for helical background turbulence, Equation (22) can be reduced to Equation (13). Therefore, the  $\alpha_{ij}^{(1)}$  tensor is directly related to the kinetic helicity. Now let us estimate the kinetic helicity for the Bell background turbulence. The contribution of the CR current to the velocity of the background turbulence is

$$\frac{\partial \mathbf{u}^{(0)}}{\partial t} \propto -\frac{1}{c\bar{\rho}} \overline{\mathbf{J}^{\text{cr}} \times \mathbf{b}^{(0)}}. \quad (23)$$

Therefore, the corresponding contribution of the CR current to the vorticity of the background turbulence is

$$\frac{\partial}{\partial t} \nabla \times \mathbf{u}^{(0)} \propto \frac{1}{c\bar{\rho}} (\overline{\mathbf{J}^{\text{cr}} \cdot \nabla}) \mathbf{b}^{(0)}. \quad (24)$$

Multiplying Equation (23) by the vorticity  $\nabla \times \mathbf{u}^{(0)}$  and Equation (24) by the velocity  $\mathbf{u}^{(0)}$  and averaging over the ensemble, we obtain

$$\begin{aligned} \frac{\partial}{\partial t} \overline{\mathbf{u}^{(0)} \cdot (\nabla \times \mathbf{u}^{(0)})} &\propto -\frac{\overline{J_j^{\text{cr}}}}{c\bar{\rho}} \overline{(\mathbf{b}^{(0)} \times (\nabla \times \mathbf{u}^{(0)}))_j} \\ &\quad - \overline{u_n^{(0)} \nabla_j b_n^{(0)}}. \end{aligned} \quad (25)$$

Dimensional reasoning yields the following estimate for the kinetic helicity for the Bell background turbulence:

$$\begin{aligned} \overline{\mathbf{u}^{(0)} \cdot (\nabla \times \mathbf{u}^{(0)})} &\propto \left( \frac{\tau^2 \overline{J_j^{\text{cr}} J_i^{\text{cr}}}}{c^2 \bar{\rho}^2} \right) \varepsilon_{jnm} \overline{b_m^{(0)} \nabla_i b_n^{(0)}} \\ &\quad + \frac{\tau \overline{J_j^{\text{cr}}}}{c\bar{\rho}} \overline{u_n^{(0)} \nabla_j b_n^{(0)}}, \end{aligned} \quad (26)$$

where we have taken into account that  $\nabla \times \mathbf{u}^{(0)} \propto (\tau/c\bar{\rho}) (\overline{\mathbf{J}^{\text{cr}} \cdot \nabla}) \mathbf{b}^{(0)}$ . The first term on the right-hand side of Equation (26) is related to the current and magnetic helicities. For the Bell instability  $\mathbf{b}^{(0)}(\mathbf{k}) \approx i(\mathbf{k} \cdot \mathbf{B}_*) \mathbf{u}^{(0)}(\mathbf{k})/\gamma_B$ . Therefore, Equations (20) and (26) show that only part of the contribution to  $\alpha_{ij}^{(1)}$  may be related to the kinetic helicity. This contribution is caused by the last term on the right-hand side of Equation (26). Note that Equation (26) for the kinetic helicity is different from Equation (C6) of Bykov et al. (2011), where no substitution for  $\mathbf{b}^{(1)}$ , as in Equation (18), is performed.

### 3.3. Large-scale Instability for $\tilde{\mathbf{B}}(t, x, y)$

Let us start to analyze the large-scale instability using a case of incompressible flow when perturbations of velocity and magnetic field are independent of  $z$ . In this case, perturbations of the mean magnetic field  $\tilde{\mathbf{B}}(t, x, y)$  are determined by the following equation:

$$\frac{\partial \tilde{\mathbf{B}}}{\partial t} = (\overline{\mathbf{B}_* \cdot \nabla}) \tilde{\mathbf{U}} + \nabla \times (\overline{\mathbf{u} \times \mathbf{b}}), \quad (27)$$

where  $(\overline{\mathbf{u} \times \mathbf{b}})_i = \alpha_{ij}^{\text{cr}} \tilde{B}_j - \eta_t (\nabla \times \tilde{\mathbf{B}})_i$ ,  $\eta_t = C_\eta u_0 \ell_0$  is the turbulent magnetic diffusivity,  $C_\eta \approx 1/3$  is a constant,  $\ell_0$  is the maximum (integral) scale of turbulent motions,  $u_0$  is

the characteristic turbulent velocity in the integral scale of turbulence, and  $\tilde{\mathbf{B}} = \tilde{\mathbf{B}}_* + \tilde{\mathbf{B}}$  and  $\tilde{\mathbf{U}}(t, x, y)$  are the perturbations of the mean velocity field. Here, for simplicity, we neglect small anisotropic contributions to the turbulent magnetic diffusion. Since the equilibrium uniform mean magnetic field  $\tilde{\mathbf{B}}_*$  is directed along the  $z$ -axis, the first term,  $(\tilde{\mathbf{B}}_* \cdot \nabla) \tilde{\mathbf{U}}$ , on the right-hand side of Equation (27) vanishes for perturbations that are independent of  $z$ . In this case the mean-field induction Equation (27) is decoupled from the mean-field momentum equation. The perturbations of the mean magnetic field  $\tilde{\mathbf{B}}$  can be written in the form of the axisymmetric field:  $\tilde{\mathbf{B}} = \tilde{B}_z(t, x, y) \mathbf{e} + \nabla \times [\tilde{A}(t, x, y) \mathbf{e}]$ .

Let us start the analysis with the simpler case in which the tensor  $\alpha_{ij}^{\text{cr}} = \alpha^{\text{cr}} \delta_{ij}$  is isotropic. Then the functions  $\tilde{B}_z(t, x, y)$  and  $\tilde{A}(t, x, y)$  are determined by the following equations, which follow from Equation (27):

$$\frac{\partial \tilde{B}_z}{\partial t} = -\alpha^{\text{cr}} \Delta \tilde{A} + \eta_t \Delta_H \tilde{B}_z, \quad (28)$$

$$\frac{\partial \tilde{A}}{\partial t} = \alpha^{\text{cr}} \tilde{B}_z + \eta_t \Delta_H \tilde{A}, \quad (29)$$

where  $\Delta_H = \nabla_x^2 + \nabla_y^2$ . We seek a solution of the mean-field dynamo Equations (28) and (29) of the form  $\propto \exp[\gamma_{\text{inst}} t + i(K_x x + K_y y)]$ . The growth rate  $\gamma_{\text{inst}}$  of the mean-field dynamo instability in homogeneous turbulent plasma with CRs is then given by

$$\gamma_{\text{inst}} = |\alpha^{\text{cr}} K| - \eta_t K^2, \quad (30)$$

where  $K^2 = K_x^2 + K_y^2$  and  $\alpha^{\text{cr}} = \alpha_1^{\text{cr}}$ . This large-scale dynamo instability is called  $\alpha^2$  dynamo, because this dynamo is caused by the interaction between two modes, toroidal,  $\tilde{\mathbf{B}}^{(T)} = \tilde{B}_z(t, x, y) \mathbf{e}$ , and poloidal mean magnetic fields, where poloidal field,  $\tilde{\mathbf{B}}^{(P)} = \nabla \times [\tilde{A}(t, x, y) \mathbf{e}]$ , is determined only by the potential  $\tilde{A}(t, x, y)$ . The toroidal field is generated from the poloidal field by the  $\alpha$  effect due to the first term,  $-\alpha^{\text{cr}} \Delta \tilde{A}$  in Equation (28), while the poloidal field is generated from the toroidal field by the  $\alpha$  effect (due to the first term,  $\alpha^{\text{cr}} \Delta \tilde{B}_z$  in Equation (29)). This implies that the  $\alpha$  effect acts twice in the positive feedback loop, and these interactions between the magnetic field components cause the  $\alpha^2$  mean-field dynamo.

Now we consider the case in which the tensor  $\alpha_{ij}^{\text{cr}}$  is anisotropic. In this case the functions  $\tilde{B}_z(t, x, y)$  and  $\tilde{A}(t, x, y)$  are given by

$$\frac{\partial \tilde{B}_z}{\partial t} = -\alpha_{yy}^{\text{cr}} \nabla_x^2 \tilde{A} - \alpha_{xx}^{\text{cr}} \nabla_y^2 \tilde{A} + \eta_t \Delta_H \tilde{B}_z, \quad (31)$$

$$\frac{\partial \tilde{A}}{\partial t} = \alpha_{zz}^{\text{cr}} \tilde{B}_z + \eta_t \Delta_H \tilde{A}, \quad (32)$$

where  $\alpha_{xx}^{\text{cr}} = \alpha_{yy}^{\text{cr}} \neq \alpha_{zz}^{\text{cr}}$ . The growth rate  $\gamma_{\text{inst}}$  of the mean-field dynamo instability in this case is

$$\gamma_{\text{inst}} = |K| \sqrt{\alpha_{yy}^{\text{cr}} \alpha_{zz}^{\text{cr}}} - \eta_t K^2, \quad (33)$$

and the ratio of magnetic energies along and perpendicular to the direction of the CR current is given by

$$\frac{\tilde{B}_z^2}{\tilde{B}_x^2 + \tilde{B}_y^2} = \frac{\alpha_{xx}^{\text{cr}}}{\alpha_{zz}^{\text{cr}}}, \quad (34)$$

where  $\alpha_{xx}^{\text{cr}} = \alpha_{yy}^{\text{cr}} = \alpha_1^{\text{cr}} + \alpha_2^{\text{cr}}$  and  $\alpha_{zz}^{\text{cr}} = \alpha_1^{\text{cr}} + 2\alpha_2^{\text{cr}}$ .

Comparing with Bykov et al. (2011), who studied a long-wave instability for incompressible flows of a plasma with CRs, we note that their growth rate vanishes when perturbations of mean magnetic and velocity fields are independent of  $z$ ; see their Equation (23). In this sense, the mean-field dynamo mechanism studied in our paper for  $K_z = 0$  is a complementary effect to a mechanism related to the long-wave instability discussed by Bykov et al. (2011).

### 3.4. Large-scale Instability for $\tilde{\mathbf{B}}(t, z)$

Now let us consider the case when perturbations of mean magnetic and velocity fields depend only on  $z$ . The perturbations  $\tilde{B}_z = 0$  (because  $\nabla \cdot \tilde{\mathbf{B}} = 0$ ) and the large-scale dynamo instability can generate magnetic field only in the direction perpendicular to the CR current. In this case we seek a solution of the linearized mean-field dynamo Equations (11) and (12) of the form  $\propto \exp(\gamma_{\text{inst}} t + i K_z z)$ . The growth rate  $\gamma_{\text{inst}}$  of the large-scale dynamo instability is given by

$$\gamma_{\text{inst}} = \left[ |\Omega_A \Omega^{\text{cr}}| - \Omega_A^2 + \frac{1}{4}(\alpha^{\text{cr}} K_z)^2 \right]^{1/2} + \frac{1}{2} |\alpha^{\text{cr}} K_z| - \eta_t K_z^2, \quad (35)$$

where  $\Omega_A = K_z \bar{V}_A$ ,  $\Omega^{\text{cr}} = c^{-1} \bar{J}^{\text{cr}} (4\pi/\bar{\rho})^{1/2}$ , and  $\alpha^{\text{cr}} = \alpha_{xx}^{\text{cr}} = \alpha_{yy}^{\text{cr}} = \alpha_1^{\text{cr}} + \alpha_2^{\text{cr}}$ . The growth rate  $\gamma_{\text{inst}}$  of the dynamo instability can be interpreted as the interaction of the  $\alpha^2$  large-scale dynamo instability (determined by the terms  $\propto \alpha^{\text{cr}} K_z$  in Equation (35)) and the Bell instability (described by the terms  $\propto |\Omega_A \Omega^{\text{cr}}| - \Omega_A^2$  in Equation (35)) in a homogeneous turbulent plasma with a CR current. When  $\alpha^{\text{cr}} = 0$ , the growth rate of the large-scale instability (35) coincides with that derived by Bykov et al. (2011); see Equation (23) of their paper.

## 4. DIRECT NUMERICAL SIMULATIONS

### 4.1. DNS Model

We consider a cubic computational domain of size  $L^3$ . The smallest wavenumber is  $k_1 = 2\pi/L$ . We adopt an isothermal equation of state with constant sound speed  $c_s$ , so the gas pressure is  $p = \rho c_s^2$ . We solve the equations of compressible MHD in the form

$$\rho \frac{D\mathbf{U}}{Dt} = \frac{1}{4\pi} (\nabla \times \mathbf{B}) \times \mathbf{B} - c_s^2 \nabla \rho + \nabla \cdot (2\nu \rho \mathbf{S}) - \frac{1}{c} \mathbf{J}^{\text{cr}} \times \mathbf{B}, \quad (36)$$

$$\frac{\partial \mathbf{A}}{\partial t} = \mathbf{U} \times \mathbf{B} + \eta \nabla^2 \mathbf{A}, \quad (37)$$

$$\frac{\partial \rho}{\partial t} = -\nabla \cdot \rho \mathbf{U}, \quad (38)$$

where  $\nu$  and  $\eta$  are kinematic viscosity and magnetic diffusivity, respectively,  $\mathbf{B} = \mathbf{B}_0 + \nabla \times \mathbf{A}$  is the magnetic field consisting of a uniform mean background field,  $\mathbf{B}_0 = (0, 0, B_0)$ , and a

nonuniform part that is represented in terms of the magnetic vector potential  $\mathbf{A}$ , and  $\mathbf{S}_{ij} = 1/2(U_{i,j} + U_{j,i}) - 1/3\delta_{ij}\nabla \cdot \mathbf{U}$  is the traceless rate of strain tensor, where commas denote partial differentiation.

In all cases we adopt triply periodic boundary conditions. The simulations are performed with the PENCIL CODE,<sup>5</sup> which uses sixth-order explicit finite differences in space and a third-order accurate time stepping method (Brandenburg & Dobler 2002). Simulations have been done with various resolutions, but here we focus on two runs with  $512^3$  mesh points. Some of the results are also compared with corresponding ones at  $256^3$  mesh points.

### 4.2. Test-field Method

We apply the quasi-kinematic test-field method (see, e.g., Schrunner et al. 2005, 2007; Brandenburg et al. 2008) to determine all relevant components of the tensor  $\alpha_{ij}$  and turbulent magnetic diffusion. This method allows for the presence of strong magnetic field as long as the magnetic fluctuations are entirely a consequence of the imposed field (Rheinhardt & Brandenburg 2010). The essence of this method is that a set of prescribed test fields  $\bar{\mathbf{B}}^{(p,q)}$  and the flow from the direct numerical simulation (DNS) are used to evolve separate realizations of small-scale fields  $\mathbf{b}^{(p,q)}$ . Neither the test fields  $\bar{\mathbf{B}}^{(p,q)}$  nor the small-scale fields  $\mathbf{b}^{(p,q)}$  act back on the flow. These small-scale fields are then used to compute the EMF  $\bar{\mathcal{E}}^{(p,q)}$  corresponding to the test field  $\bar{\mathbf{B}}^{(p,q)}$ . The number and form of the test fields used depend on the problem at hand.

The choice of test fields depends on the averaging that is performed. Relevant for the present study are averages that depend on  $x$  or  $y$ , or both. To gather sufficient statistics, we adopt planar  $yz$  averages that depend on  $x$ , so we use test fields  $\bar{\mathbf{B}}^{(1c)} = (0, \tilde{B}_0 \cos kx, 0)$ ,  $\bar{\mathbf{B}}^{(1s)} = (0, \tilde{B}_0 \sin kx, 0)$ ,  $\bar{\mathbf{B}}^{(2c)} = (0, 0, \tilde{B}_0 \cos kx)$ , and  $\bar{\mathbf{B}}^{(2s)} = (0, 0, \tilde{B}_0 \sin kx)$ , in which case the series expansion of the EMF contains two terms,

$$\mathcal{E}_i = a_{ij} \bar{B}_j - \eta_{ij} (\nabla \times \bar{\mathbf{B}})_j. \quad (39)$$

The symmetric part of the tensor  $a_{ij}$  is of particular interest and is commonly referred to as the  $\alpha$  tensor,

$$\alpha_{ij} = \frac{1}{2}(a_{ij} + a_{ji}). \quad (40)$$

Errors are estimated by dividing the time series into three equally long parts and computing time averages for each of them. The largest departure from the time average computed over the entire time series represents an estimate of the error.

### 4.3. DNS Results

All runs are isothermal with  $c_s = 10$ . The box has a size of  $16\pi$ , i.e.,  $k_1 = 1/8$ . In our units,  $\rho_0 = 1$ , and the magnetic Prandtl number  $\nu/\eta = 1$ . The relevant non-dimensional parameters are  $\text{Lu} = v_{A0}/\eta k_1$  (the Lundquist number), where  $v_{A0} = B_0$  is the non-dimensional Alfvén speed, and  $\mathcal{J} = 4\pi J^{\text{cr}}/c B_0 k_1$  (the non-dimensional CR current density).

Visualizations of the magnetic field  $B_x/B_0$  on the periphery of the computational domain are shown in Figure 1 for a run with  $512^3$  mesh points using the following parameters: the non-dimensional CR current density is  $\mathcal{J} = 80$  and the Lundquist number  $\text{Lu} = 80$  (with  $J^{\text{cr}} = 0.1$ ,  $B_0 = 0.01$ , and  $k_1 = 1/8$ ). In the beginning of the instability, the length scale is rather

<sup>5</sup> <http://pencil-code.googlecode.com>

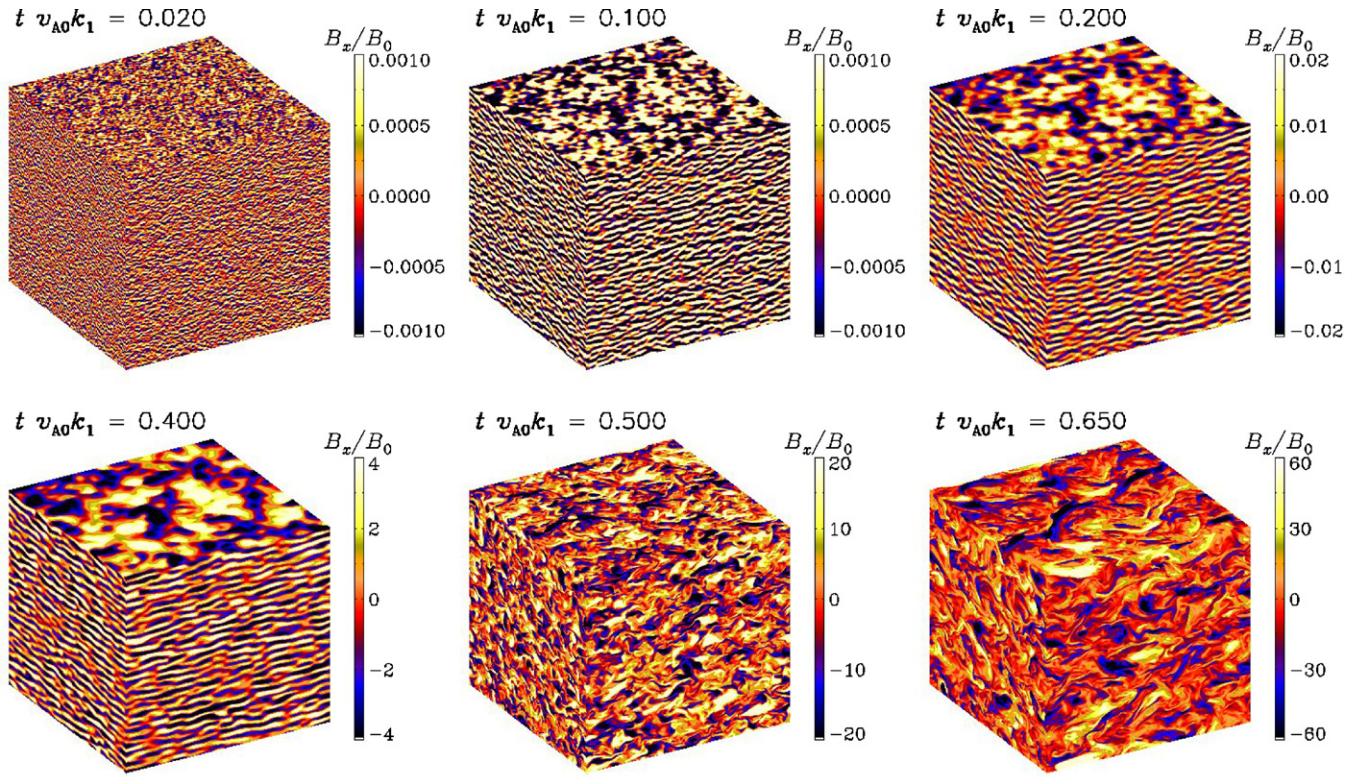


**Figure 1.** Visualization of  $B_x/B_0$  on the periphery of the computational domain using  $512^3$  mesh points for  $J^{\text{cr}} = 0.1$ ,  $B_0 = 0.01$ ,  $k_1 = 1/8$  (so that  $\mathcal{J} = 80$ ), and  $\nu = \eta = 10^{-3}$  (so that the Lundquist number  $\text{Lu} = 80$ ).

(A color version of this figure is available in the online journal.)

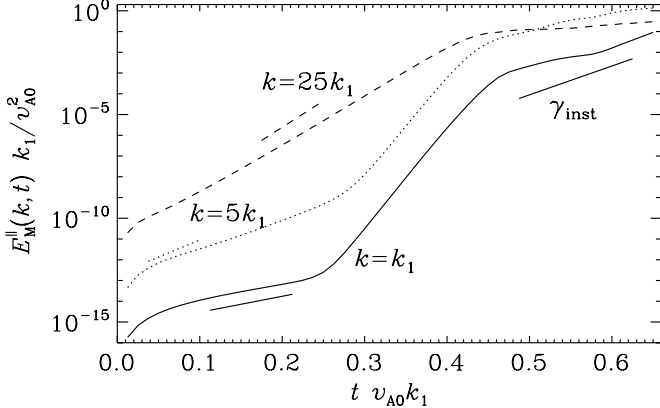


**Figure 2.** Time evolution of  $E_M^{\parallel} k_1 / v_{A0}^2$  for modes with different wavenumbers for the run with  $\mathcal{J} = 80$ . The short straight lines show the growth rate of the Bell instability, as given by Equation (9) for modes with three selected values of  $k$ , as well as the value of  $\gamma_{\text{inst}}$  as given by Equation (33).

small, but it increases continuously as time goes on. Note in particular the much larger horizontal length scales in the  $xy$  plane that may be associated with the dynamo instability. After  $t v_{A0} k_1 \approx 0.5$ , the instability reaches yet another stage during which the magnetic field pattern becomes turbulent. Again, as time goes on, the typical eddy scale increases.

All runs with a constant CR current show that there is a growth until the velocities become eventually supersonic. This is probably the reason the simulation terminates. It is conceivable that this could be avoided by including the back-reaction of the amplified field on the CR current, which would limit the Bell instability (Riquelme & Spitkovsky 2009). In Figures 2 and 3, we show the time evolution of the normalized spectral vertical

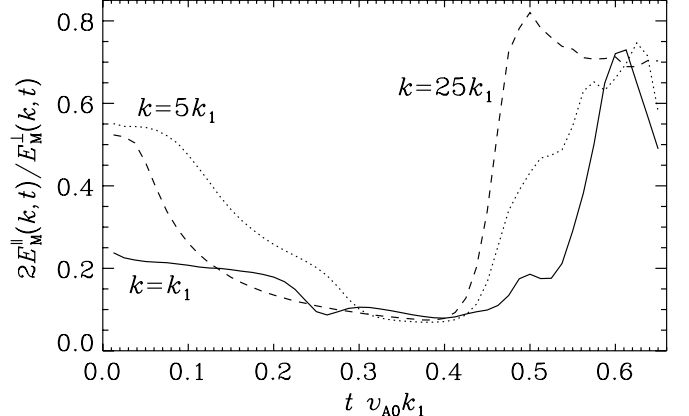


**Figure 3.** Time evolution of the ratio of the spectral vertical (along the imposed field  $B_0$ ) and horizontal magnetic energies  $2E_M^{\parallel} / E_M^{\perp}$  for the run with  $\mathcal{J} = 80$ .

magnetic energies  $E_M^{\parallel} k_1 / v_{A0}^2$  and the ratio of the spectral vertical (along the imposed field  $B_0$ ) and horizontal magnetic energies  $2E_M^{\parallel} / E_M^{\perp}$  for modes with different wavenumbers for the same run as in Figure 1. As follows from these figures, the dynamics of the instability has the following stages:

1. In the early stage there is the development of small-scale instability that results in the production of small-scale turbulence. It is seen in Figure 2 that the mode-averaged growth rate of this instability in this stage is slightly smaller than that of Equation (9) that describes the Bell instability for the fastest growing mode of a given  $|k|$ , as should be expected.
2. In the second stage, there is formation of large-scale magnetic structures (during the interval 0.2–0.4 Alfvén

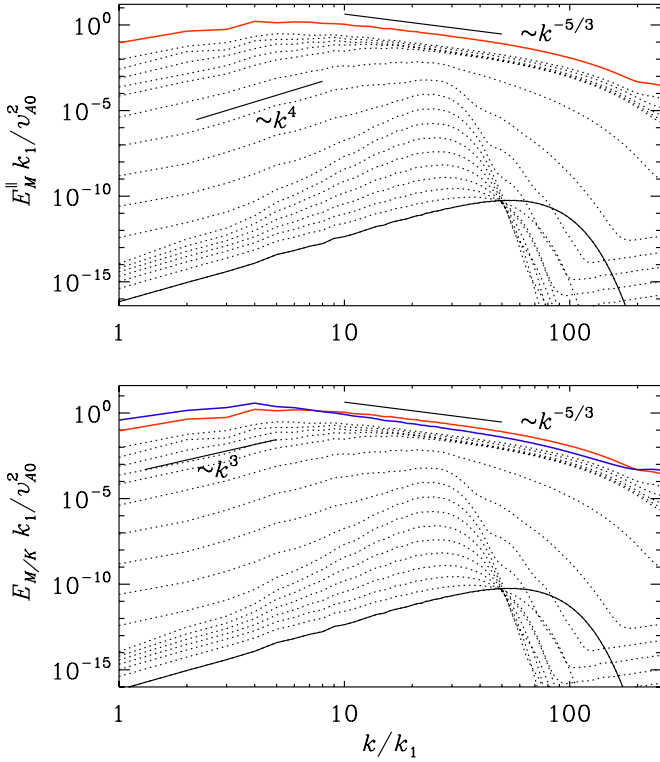


**Figure 4.** Time evolution of  $E_M^\parallel$  and  $E_M$  for the run using  $512^3$  mesh points ( $J^{\text{cr}} = 0.1$ ,  $B_0 = 10^{-2}$ , so that  $\mathcal{J} = 80$ ). The normalized time interval between different spectra is  $v_{A0} k_1 \Delta t = 3/80 \approx 0.04$ . The solid lines refer to the initial spectra proportional to  $k^4$  for small values of  $k$ , and the red and blue lines represent the last instant of  $E_M$  and  $E_K$ , respectively. The straight lines show the  $k^4$  and  $k^{-5/3}$  power laws.

(A color version of this figure is available in the online journal.)

times; see Figure 1). Note from Figure 2 that the growth rate of the large-scale mode  $k = k_1$  is about twice the growth rate of the largest mode. The interpretation of this will be given below.

3. In the final stage, there is a development of larger-scale turbulence; the perturbed field actually exceeds the original field by a considerable factor, and a significant fraction of the energy is now present in modes with  $k_\perp \simeq k_\parallel$ . The growth rate in this final stage agrees with that predicted by Equation (33), where  $\alpha_{yy}^{\text{cr}}$ ,  $\alpha_{zz}^{\text{cr}}$ , and  $\eta_t$  have been obtained with the test-field method, as described below.

Time evolution of power spectra of magnetic energy of the  $B_z$  component,  $E_M^\parallel$ , and those of all components,  $E_M$ , are shown in Figure 4, which demonstrates an inverse energy cascade-like behavior. The evolution during the second stage (during the interval 0.2–0.4 Alfvén times; see Figure 1) shows that large-scale modes ( $k \sim k_1$ ) are growing at about *twice* the growth rate of the fastest growing mode  $k/k_1 \sim 25$ . We interpret this as perturbation field growth  $\partial b/\partial t$  at large scale due to the coupling of pairs of higher- $k$  modes ( $k_1$  and  $k_2$ , say), and therefore proportional to  $u_{\text{rms}}^2 B_0 \propto \exp(\gamma_1 + \gamma_2)$ , where  $\gamma_1$  and  $\gamma_2$  are the respective linear growth rates of the high- $k$  modes. During this stage, the perturbed field is still small compared to the original field, so the exponential growth of the total field as described by Equations (13) and (14) has not yet begun.

At the end of the simulation, both kinetic and magnetic energy spectra develop a  $k^{-5/3}$  energy spectrum. This is shown in Figure 5, where we plot spectra compensated by  $\epsilon^{-2/3} k^{5/3}$ ,

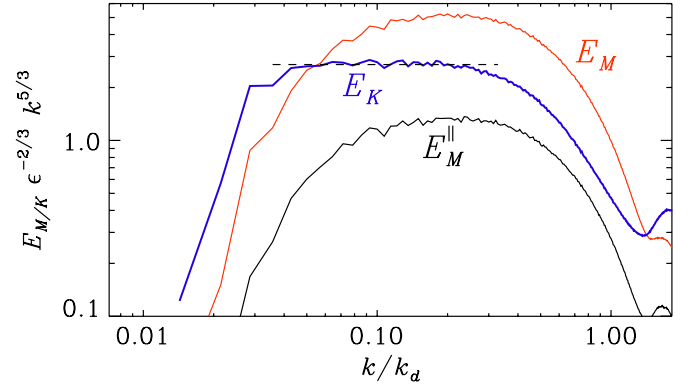


**Figure 5.** Compensated spectra of  $E_K$  (blue),  $E_M$  (red), and  $E_M^\parallel$  (black), at the end of the simulation. Here,  $\epsilon$  is the total (kinetic and magnetic) energy dissipation rate. The dashed horizontal line goes through 2.7.

(A color version of this figure is available in the online journal.)

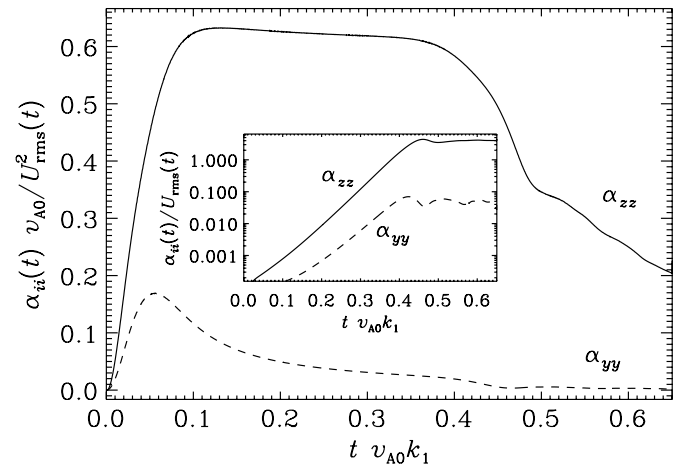


**Figure 6.** Normalized  $\alpha_{zz} v_{A0}/u_{\text{rms}}^2$  and  $\alpha_{yy} v_{A0}/u_{\text{rms}}^2$  for the run with  $\mathcal{J} = 80$ . The inset shows that after about 0.45 Alfvén times, both  $\alpha_{yy}^{\text{DNS}}/u_{\text{rms}}$  and  $\alpha_{zz}^{\text{DNS}}/u_{\text{rms}}$  are approximately constant in time.

where  $\epsilon$  is the total (kinetic and magnetic) energy dissipation rate. The wavenumber is normalized by the dissipation wavenumber  $k_d = [\epsilon/(\nu + \eta)]^{3/4}$ .

The test-field results for the normalized components of the  $\alpha$  tensor,  $\alpha_{zz} v_{A0}/u_{\text{rms}}^2$  and  $\alpha_{yy} v_{A0}/u_{\text{rms}}^2$ , are shown in Figure 6 for the same run. The value of  $\alpha_{zz}^{\text{DNS}} v_{A0}/u_{\text{rms}}^2 \approx 0.6$  is of the same order of magnitude as that determined by Equation (14), i.e.,  $\alpha_{zz}^{\text{theory}} v_{A0}/u_{\text{rms}}^2 \approx 0.5$ . Note that at late times, after about 0.45 Alfvén times, we find that both  $\alpha_{yy}^{\text{DNS}}/u_{\text{rms}}$  and  $\alpha_{zz}^{\text{DNS}}/u_{\text{rms}}$  are approximately constant in time. This measured value of the  $\alpha$  effect is much larger than that based on kinetic helicity determined by Equation (13), unless  $\tau_0$  is considerably larger than  $1/ku_{\text{rms}}$  (see Figure 7). We interpret this as evidence for an additional contribution, Equation (14). The growth rate of the large-scale dynamo instability is of the same order as that theoretically predicted from the large-scale dynamo instability. Indeed, Equation (33) for the growth rate yields  $\gamma^{\text{theory}} \approx 0.03$ , corresponding to  $\gamma^{\text{theory}}/v_{A0} k_1 \approx 24$  in non-dimensional units. This value is in agreement with the growth rate expected from an  $\alpha^2$  dynamo with coefficients obtained with the test-field method; see the inset of Figure 7, where  $\gamma_{\text{inst}}/v_{A0} k_1 \approx 20$ . This agrees with the growth seen in the DNS at  $k = k_1$  during the time interval 0.45–0.65; see Figure 2. Finally, Equation (34) for the ratio of magnetic energies along and perpendicular to the

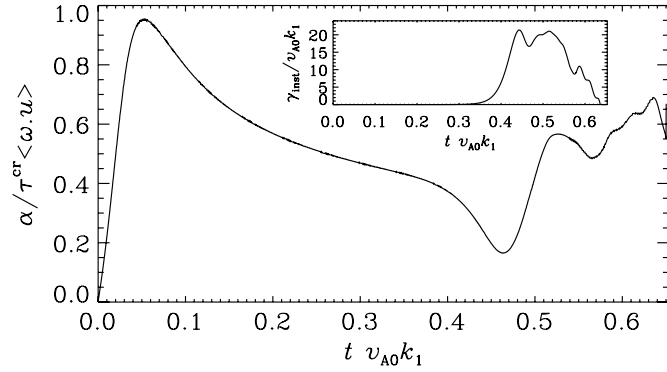


**Figure 7.** Evolution of  $\alpha = (\alpha_{yy}\alpha_{zz})^{1/2}$ , normalized by  $\tau^{\text{cr}}(\omega \cdot \mathbf{u})$ , where  $\tau^{\text{cr}} = 1/\omega^{\text{cr}}$  for the run with  $\mathcal{J} = 80$ . The inset gives the instantaneous value of  $\gamma_{\text{inst}}$  as derived from Equation (33).

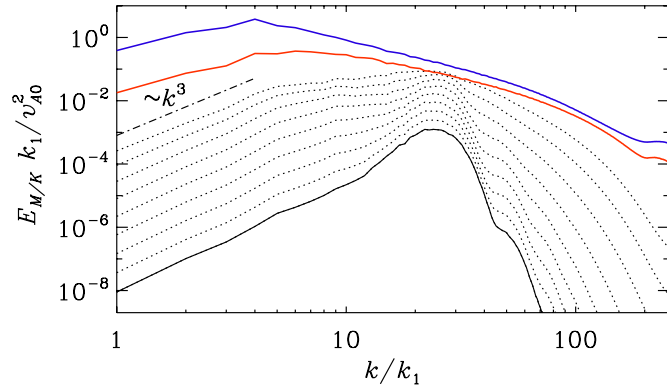


**Figure 8.** Same as the bottom panel of Figure 4 ( $\mathcal{J} = 80$ ), but showing only the time interval  $0.35 \leq t v_{A0} k_1 \leq 0.45$  (dashed lines), i.e., the last 0.1 Alfvén times just near the end of the linear growth phase. The black solid lines refer to  $t v_{A0} k_1 = 0.35$ , while red and blue lines refer to  $k_f^M(t)$  and  $k_f^K(t)$ , respectively, at  $t v_{A0} k_1 = 0.65$ . The slope  $k^3$  is shown for comparison.

(A color version of this figure is available in the online journal.)

direction of the CR current yields  $[\tilde{B}_z^2 / (\tilde{B}_x^2 + \tilde{B}_y^2)]^{\text{theory}} \approx 0.08$ , while this ratio according to DNS (see Figure 3) is estimated as  $[\tilde{B}_z^2 / (\tilde{B}_x^2 + \tilde{B}_y^2)]^{\text{DNS}} \approx 0.06$ . The above comparison is a good agreement between theoretical predictions and the results of the numerical simulations.

In Figure 8, we show the time evolution of power spectra of magnetic energy of the  $B_z$  component,  $E_M^{\parallel}$ , and those of all components,  $E_M$ , like it was presented in Figure 4, but during only the last 1/10 of an Alfvén time. We see that the amplification of magnetic field with respect to initial perturbations during the last 1/10 of an Alfvén time (which is of the order of the shock crossing time) at  $k = k_1$  is 3.5 orders of magnitude (i.e., up to  $0.6 \times 10^{-3}$  of the field). However, this field is less than the equilibrium-imposed field  $B_0 = 10^{-2}$ . On the other hand, the visualizations of the magnetic field  $B_x/B_0$  on the periphery of the computational domain shown in Figure 1 demonstrate that the ratio  $B_x/B_0 < 60$  at  $t v_{A0} k_1 = 0.65$ .

To quantify the inverse cascade-like behavior, let us now look at the evolution of the wavenumber of the magnetic-energy-carrying eddies,  $k_f^M$ , defined via

$$[k_f^M(t)]^{-1} = \int k^{-1} E_M(k, t) dk / \int E_M(k, t) dk, \quad (41)$$

and likewise for kinetic energy and magnetic energy in the  $z$  component,  $k_f^K$  and  $k_f^{M\parallel}$ , respectively (see Figure 9). It turns out

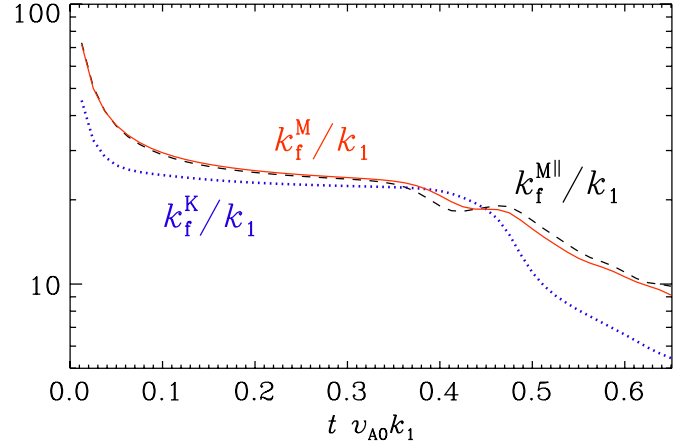


**Figure 9.** Evolution of  $k_f^M$  (solid, red),  $k_f^{M\parallel}$  (dashed), and  $k_f^K$  (dotted, blue) for the same run as in Figure 1 ( $\mathcal{J} = 80$ ).

(A color version of this figure is available in the online journal.)

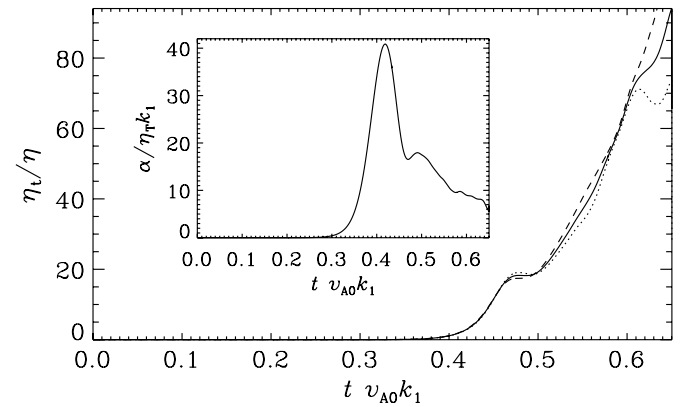


**Figure 10.** Evolution of  $\eta_t/\eta$  (solid line),  $\eta_{yy}/\eta$  (dotted line), and  $\eta_{zz}/\eta$  (dashed line) for the run  $\mathcal{J} = 80$ . The inset shows  $\alpha/\eta_T k_1$ .

that all three wavenumbers reach a value somewhat above  $20 k_1$  by the end of the small-scale dynamo instability and then drop rapidly in the mean-field dynamo stage. Note, however, that the decrease of  $k_f^K$  is somewhat faster than that of  $k_f^M$ .

The test-field method yields not only  $\alpha_{ij}$  but also the components of the turbulent magnetic diffusivity tensor  $\eta_{ij}$ . It turns out that  $\eta_{yy} \approx \eta_{zz}$ . The ratio  $\eta_t/\eta$ , where  $\eta_t = (\eta_{yy} + \eta_{zz})/2$ , greatly exceeds unity in the late stages; see Figure 10. Mean-field dynamo efficiency depends on the dynamo number  $D = (\alpha/\eta_T k_1)^2$ , where  $\alpha = (\alpha_{yy}\alpha_{zz})^{1/2}$  and  $\eta_T = \eta_t + \eta$ . The dynamo number exceeds the critical value for dynamo action of unity ( $D > 1$ ) after about 0.3 Alfvén times; see the inset of Figure 10.

#### 4.4. Comparison with the Run $\mathcal{J} = 800$

In this subsection, we discuss the results of DNS with the higher CR current, i.e., when the normalized CR current is increased by one order of magnitude  $\mathcal{J} = 800$  (i.e.,  $J^{\text{cr}} = 1$ ,  $B_0 = 0.01$ , and  $k_1 = 1/8$ ), and the other parameters are the same as in the previous subsection (the Lundquist number  $\text{Lu} = 80$  and the resolution is  $512^3$  mesh points). In this case, very small scales (higher- $k$  modes) are not well resolved. On the other hand, the main contribution to the mean-field dynamo (which is the main subject of our study) is of the maximum scale of turbulent motions. The time evolution of spectra of magnetic,  $E_M$ , and kinetic,  $E_K$ , energies for  $\mathcal{J} = 800$  is shown in Figure 11,

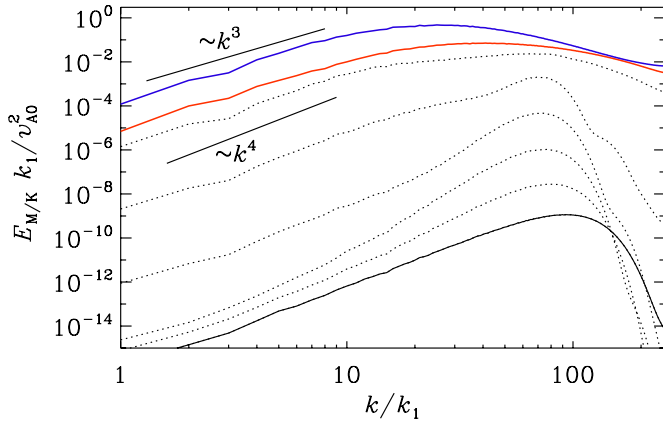


**Figure 11.** Time evolution of  $E_M$  and  $E_K$  for the run  $\mathcal{J} = 800$  ( $J^{\text{cr}} = 1$ ,  $B_0 = 10^{-2}$ ) showing only the time interval  $0.0125 \leq t v_{A0} k_1 \leq 0.075$ . The time interval between the lines  $\Delta t v_{A0} k_1 = 0.0125$ . The red and blue lines represent the last instant of  $E_M$  and  $E_K$ , respectively. The slopes  $k^4$  and  $k^3$  are shown for comparison.

(A color version of this figure is available in the online journal.)

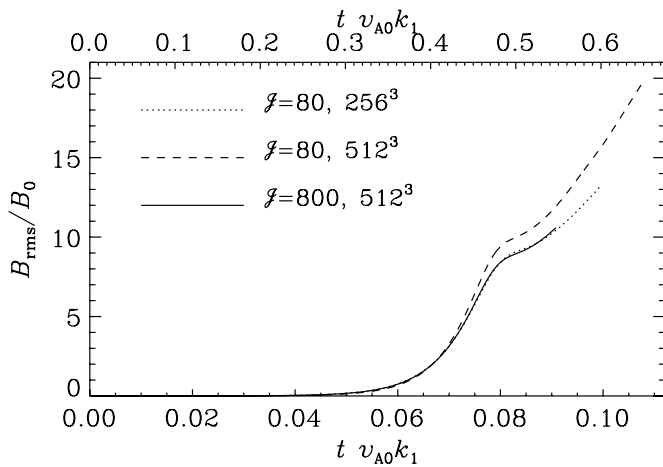


**Figure 12.** Normalized  $B_{\text{rms}}/B_0$  for runs with  $\mathcal{J} = 80$  (using  $256^3$  and  $512^3$  meshpoints; dotted and dashed lines, respectively) and  $\mathcal{J} = 800$  ( $512^3$  meshpoints, solid line). Upper horizontal axis corresponds to case  $\mathcal{J} = 80$ , while lower horizontal axis corresponds to case  $\mathcal{J} = 800$ .

demonstrating an inverse energy cascade-like behavior, but to a lesser extent in comparison with the lower CR current ( $\mathcal{J} = 80$ ).

For comparison with the case  $\mathcal{J} = 80$ , in Figures 12–14 we show the time evolution of the total magnetic field  $B_{\text{rms}}/B_0$ ,  $B_{\text{rms}}/\rho^{1/2} U_{\text{rms}}$  (which does not include the imposed field  $B_0$ ), and the growth rate of the total velocity field,  $\gamma^{\text{DNS}} = d \ln U_{\text{rms}}/dt$ , for runs with  $\mathcal{J} = 80$  (dotted and dashed lines for  $256^3$  and  $512^3$  meshpoints, respectively) and  $\mathcal{J} = 800$  (solid line). Since the time evolution for different values of the CR current occurs on different timescales, we use the upper horizontal axis for the case  $\mathcal{J} = 80$ , while the lower horizontal axis corresponds to case  $\mathcal{J} = 800$ .

Inspection of Figure 12 shows that, at the final stage of evolution, the generated magnetic field is one order of magnitude larger than the imposed field  $B_0$ . The  $\mathcal{J} = 80$  results at lower resolution are similar to those at higher resolution, but have run for a slightly shorter time before resolution problems occurred. The growth rate of the velocity and magnetic field is five times larger for the case of  $\mathcal{J} = 800$  (see the upper panel of Figure 14). On the other hand, the evolution of the kinetic energy—apart from this rescaling of time—is not strongly dependent on the

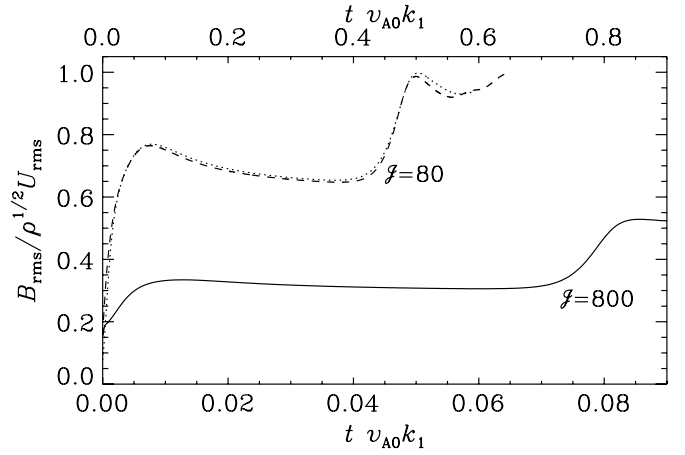


**Figure 13.** Evolution of  $B_{\text{rms}}/\rho^{1/2} U_{\text{rms}}$  for runs with  $\mathcal{J} = 80$  (dotted and dashed lines for  $256^3$  and  $512^3$  meshpoints, respectively) and  $\mathcal{J} = 800$  (solid line,  $512^3$  meshpoints). Upper horizontal axis corresponds to case  $\mathcal{J} = 80$ , while lower horizontal axis corresponds to case  $\mathcal{J} = 800$ .

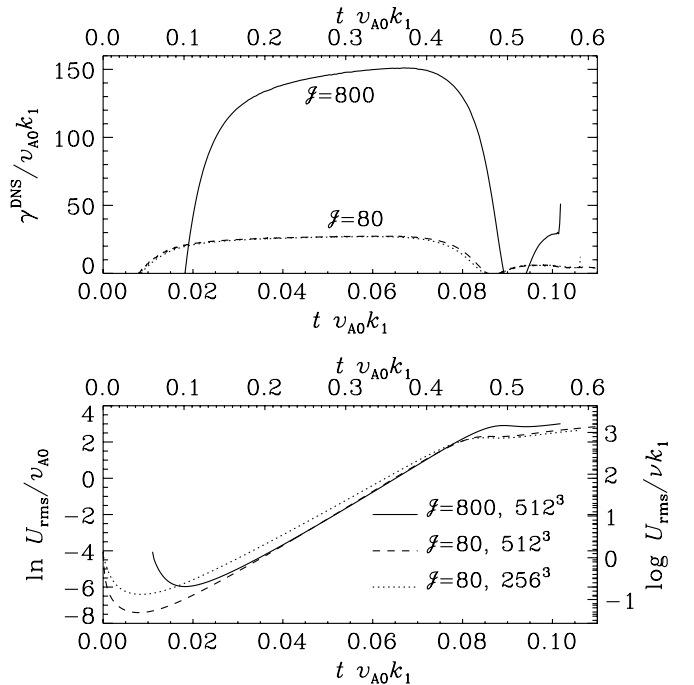


**Figure 14.** Instantaneous growth rate  $\gamma^{\text{DNS}} = d \ln U_{\text{rms}}/dt$  (upper panel) and  $\ln U_{\text{rms}}/v_A k_1$  (lower panel) for runs with  $\mathcal{J} = 80$  (dotted and dashed lines for  $256^3$  and  $512^3$  meshpoints, respectively) and  $\mathcal{J} = 800$  (solid line,  $512^3$  meshpoints). Upper horizontal axis corresponds to case  $\mathcal{J} = 80$ , while lower horizontal axis corresponds to case  $\mathcal{J} = 800$ .

CR current (see the lower panel of Figure 14), and neither is  $\alpha_{zz}/U_{\text{rms}}$  (see the test-field results of the measured  $\alpha$  effect in Figure 15 shown in log scale).

As noted above, the quasi-kinematic test-field method is valid as long as the magnetic fluctuations are entirely a consequence of the imposed field. In one particular case we have verified this by comparing with results from a fully nonlinear test-field method where velocity fluctuations resulting from the interaction with magnetic field fluctuations are also included. This method has currently been tested and implemented in the PENCIL CODE only for a modified set of equations in which the pressure gradient and the  $\mathbf{U} \cdot \nabla \mathbf{U}$  term are omitted, but the Lorentz force is fully retained (Rheinhardt & Brandenburg 2010). We

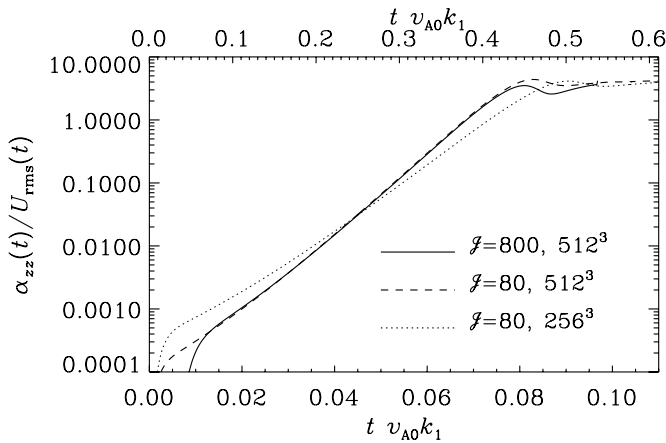


**Figure 15.** Normalized  $\alpha_{zz}/U_{\text{rms}}$  for runs with  $\mathcal{J} = 80$  (dotted and dashed lines for  $256^3$  and  $512^3$  meshpoints, respectively) and  $\mathcal{J} = 800$  (solid line,  $512^3$  meshpoints). Upper horizontal axis corresponds to case  $\mathcal{J} = 80$ , while lower horizontal axis corresponds to case  $\mathcal{J} = 800$ .

have applied this method, with the modified set of equations, to a case similar to that displayed in Figure 6, but at lower resolution ( $64^3$ ). In that case,  $\alpha_{yy}v_A/U_{\text{rms}}^2$  is nearly constant after  $t v_A k_1 = 0.1$  and comparable to the corresponding value shown in Figure 6 at  $t v_A k_1 = 0.4$ , while  $\alpha_{zz}v_A/U_{\text{rms}}^2$  agrees with that of Figure 6 in the full time interval. More importantly, however, the quasi-kinematic and fully nonlinear test-field methods agree with each other within machine precision, confirming thus the applicability of the quasi-kinematic method to the present case.

#### 4.5. Interpretation of the Results

Our results seem consistent with the following interpretation. There appear to be three distinct stages. In the first stage, the  $c^{-1} \mathbf{J}^{\text{cr}} \times \mathbf{b}$  force (which we refer to as the Lorentz force due to the “counter-CR current”—i.e., the current in the thermal plasma that cancels the CR current) amplifies the motion perpendicular to the original, unperturbed magnetic field in one circular polarization of Alfvén modes, thereby stretching the field such that it develops a component that is perpendicular to the original direction. This is the Bell instability in our simulation, but anything that creates a perpendicular component might work just as well for this phase. The Bell instability grows fastest on small scales and in a direction whose  $\mathbf{k}$  vector is parallel to the  $z$ -axis. Tentatively, we may attribute the increasing preference for “perpendicular” energy that we see in the simulation, i.e., energy in motion in the “perpendicular” ( $x$  and  $y$ ) directions, to the faster growth rate of on-axis ( $k = k_z$ ) Alfvén waves. However, there is clearly significant parallel energy, even in the linear growth regime, presumably due to off-axis waves. The reason that the ratio of “parallel” to “perpendicular” energy decreases in the first stage is presumably because the on-axis waves, which have only motion perpendicular to the axis, are the fastest growing modes.

During the first stage, the ratio of  $\alpha_{zz}$  to  $u_{\text{rms}}$  grows exponentially, because for any given mode,  $\alpha \propto \mathbf{u} \cdot \nabla \times \mathbf{u} \sim k u^2$  is proportional to  $u^2$ , and  $\mathbf{u}$  is growing exponentially (Figure 14), consistent with the linear Bell instability. The correlation length of both the magnetic field and the turbulence, apart from a drop in the very early stages, remains more or less constant and corresponds to the scale of the fastest growing modes.

The second stage is much like the first, except that the growth rate of the larger-scale, low- $k$  modes begins to increase above

its linear value; see Figure 2. This is presumably due to the fact that their growth is dominated by nonlinear coupling of higher- $k$  modes, which have developed much larger amplitudes than the low- $k$  ones, even though they are still in the linear regime.

The third stage, for  $\mathcal{J} = 80$  ( $\mathcal{J} = 800$ ), begins at about  $t v_{A0} k_1 \sim 0.45$  ( $t v_{A0} k_1 \sim 0.06$ ), as shown in the upper panel of Figure 14. Several things clearly happen at the onset of the second stage: (1) the growth of  $U_{\text{rms}}$  suddenly slows (Figure 14); (2) the growth of the magnetic field also shows a change (Figure 12), though it continues to rise; (3) the *correlation lengths* of both the magnetic field and the velocity begin to increase noticeably (Figure 9); (4) the ratio of  $\alpha$  to  $u_{\text{rms}}$  stops rising exponentially and either flattens out or grows much more slowly (Figures 6 and 15); (5) the turbulent magnetic diffusivity begins to rise significantly and dominates the microscopic value (Figure 10); (6) the ratio of energy in parallel magnetic field to that in perpendicular field rises sharply (Figure 3); and (7) a Kolmogorov-type spectrum is reached from below, while the level of turbulence grows more slowly.

All these changes can be understood in terms of nonlinear effects. Once the turbulent velocity exceeds the Alfvén velocity, the nonlinear convective term in the Navier–Stokes equation becomes as important as or more important than the Lorentz force due to the counter-CR current, so that the stirring of the fluid by the latter, as expressed in unstable Alfvén modes, is in equilibrium with eddy viscosity. By the same token, the amplitude of the magnetic field is large, so that the  $\alpha^2$  dynamo is activated. Taken in isolation, an exponentially growing  $\alpha$  effect would lead to super-exponential growth, but this is not what is seen. The sudden rise of parallel to perpendicular magnetic energy could perhaps be attributed to this effect, but, looking at the shape of the spectra in Figures 4 and 11, and as said before, nonlinear mode coupling to the fastest growing modes, which here turn out to be at  $k/k_1 \approx 25$  and  $70$ , respectively, is a likely explanation.

In this *nonlinear stage*, the ratio of parallel to perpendicular energy begins to grow, and the field attains larger scale and becomes more isotropic, as can be seen in Figure 1. The  $\alpha^2$  dynamo can be interpreted as an inverse cascade, in which parallel and anti-parallel magnetic fluxes are generated by the stretching of perpendicular flux, while the anti-parallel flux is kinematically “pumped” out of any given finite region of size  $L$  at a velocity of order  $\alpha$  by the  $\alpha$  effect. The pumping of flux into large regions of size  $L$  can be viewed from a modal point of view as inverse cascading of energy into small wavenumbers of order  $\pi/L$ .

The observed scaling of the time evolution with  $\mathcal{J}$  is reasonable: the timescale for  $\mathcal{J} = 800$  is about a factor of  $5.5 \sim 10^{0.75}$  times less than that for  $\mathcal{J} = 80$ . Because the stirring force of the counter-CR current is proportional to  $\mathcal{J}$ , one might expect velocities to scale as  $\mathcal{J}$  for a fixed correlation time. However, if an acceleration  $a$  operates over a set distance  $s$ , then the velocity scales only as  $(sa)^{1/2}$ . Once the turbulent velocity exceeds  $v_{A0}$ , the amplitude of the transverse motion associated with a given mode is  $\sim 2\pi/k$ , and the correlation length varies more weakly than the correlation time with  $\mathcal{J}$ . So we expect that the timescale for the dynamo mechanism scales as  $\mathcal{J}^\delta$ , where  $0.5 \leq \delta \leq 1$ , and this is what we observe:  $\delta \simeq 0.75$ . We have not verified how this scaling law extends to larger  $\mathcal{J}$ .

In Kolmogorov turbulence, the turbulent kinetic energy  $\int E_K(k) dk$  at any instant is proportional to  $P^{2/3}$ , where  $P$  is the stirring power. In a situation such as the present one, where the stirring force  $F$  is proportional to  $\mathcal{J}B$ , for a given stirring

scale  $k$ , the velocity  $U$  scales as  $(F/k)^{1/2}$ , the power is proportional to  $F^{3/2}$ , and the energy should then, by dimensional arguments, have a finite, steady state value that is proportional to  $F$ . The point is that for a given  $B$ , the energy  $E$  has a finite value to which it should rise and flatten out. There is indication of this in our simulation results, as seen in Figures 2 and 3, where the total turbulent energy flattens out at  $t v_{A0} k_1 = 0.45$  for  $\mathcal{J} = 80$  ( $t v_{A0} k_1 = 0.08$  for  $\mathcal{J} = 800$ ). It does not completely flatten out though, and we attribute this to the fact that  $B_{\text{rms}}$  is still creeping up with time due to the dynamo effect. Our simulations are not long enough to determine whether the magnetic energy  $E_M$  always reaches equipartition with the kinetic energy  $E_K$ . If it does, then, because  $B$  scales as  $E_M^{1/2}$ , dimensional arguments suggest that the force  $F$ , which scales as  $\mathcal{J}B$ , therefore scales as  $\mathcal{J}E_K^{1/2}$ . So, if  $U$  scales as  $(F/k)^{1/2}$  and thus  $E_K$  scales as  $F$ , then the force scales as  $\mathcal{J}^2$ . We believe that it would take longer simulation runs that were currently feasible to check this prediction and whether  $E_M$  indeed scales as  $E_K$ .

In the above discussion, we have invoked the Bell instability to generate magnetic flux that is perpendicular to the local background, because this, from the point of view of the fluid, is an MHD effect and can be represented in an MHD simulation. We note, on the other hand, that non-MHD effects could achieve the same result. For example, the non-resonant firehose instability could achieve the same stretching. The helicity that is required for the  $\alpha$  effect relies on preferential growth of one circular polarization over the other, so the firehose instability on large scales, which has no such preference, could not by itself bring about an  $\alpha$  effect. However, it could combine with the resonant cyclotron instabilities to do so. In this case, the firehose instability would play the role that differential rotation plays in the  $\alpha\Omega$  dynamo—that of creating a perpendicular field component, while the helical turbulence that is generated by the Bell instability would play the role of helical turbulence that, in the  $\alpha\Omega$  dynamo, is generated by the combination of convection in a stratified medium and Coriolis force.

## 5. ASTROPHYSICAL APPLICATIONS

In a real astrophysical system, there is a limited amount of time available. In the case of an expanding blast wave, this is of order the expansion time. Similarly, in an accretion shock, accreting matter continuously sweeps magnetic field downward over the crossing timescale of the accreting matter. The question is whether this is enough for significant magnetic field amplification.

### 5.1. Blast Waves

In our simulations, the growth up to maximum amplitude takes on the order of 0.45 (0.08) Alfvén crossing times across the box for  $\mathcal{J} = 80$  ( $\mathcal{J} = 800$ ); see Figures 11–14. However, this total time interval witnesses a gain of many orders of magnitude of the level of large-scale magnetic field, because the simulation begins at the noise level. For  $\mathcal{J} = 80$  it can be seen from Figures 2 and 4 that at  $v_{A0} k_1 t \sim 0.3$ , the growth at large scales speeds up, the energy in field perturbations at any given scale grows by a factor of  $\sim 10^{3/2}$  per  $\Delta t \sim 0.04 v_{A0} k_1$ , and, at somewhat later times, by a factor of nearly  $10^2$  per  $\Delta t \sim 0.04 v_{A0} k_1$ , suggesting that, during a period of exponential growth, the gain factor over an interval  $T$  at wavenumber  $k$  is  $G(T, k) = 10^{2v_{A0} k_1 T / 0.04}$ . For an SNR of radius  $R$ , the precursor has a width  $W$  of somewhat less than  $R$ , and the largest mode has

a wavenumber of order  $k_1 = 2\pi/W \gtrsim 1$ . Thus, the available time  $T$  for field amplification by CR current is  $T = W/u_s \sim 2\pi/(k_1 v_A M_A)$ , where  $M_A = u_s/v_A$  is the Alfvén Mach number of the blast wave. Then  $v_A k_1 T \sim 2\pi/M_A$ , suggesting that the  $\alpha$  dynamo effect could amplify the field energy of the remnant by a gain factor  $G$  of order  $G = 10^{\pi/0.01 M_A}$ , and the amplification of the field’s magnitude would be the square root of this factor, i.e., a factor of several for  $M_A \sim 10^2$ . This appears to be consistent with Figure 13. According to Equation (1), and assuming  $P^{\text{cr}} \propto u_s^2$ , we see that raising the potential CR current by  $\zeta^3$  speeds up the time evolution of the field amplification by  $\zeta^\delta$ , where  $\delta$  is between 0.5 and 1; see the discussion above. So, in very young SNRs, where  $\mathcal{J}$  can be much higher than in the runs we made, the gain factor for an expansion time could be higher. In Figure 4, for example, the magnetic energy on any given scale,  $[E_K(k)k]/(k_1/k)$ , reaches, but does not significantly exceed, unity.

For young, expanding SNRs  $M_A$  is typically  $10^2$ , so the growth factor on the scale of the supernova could be of order one  $e$ -fold per expansion time if the assumptions of the simulation were to remain valid over the full interval. While not dramatic, neither is it insignificant in view of the uncertainties, a modest amount of magnetic field amplification may take place within an expanding SNR, and this may be enough to be compatible with observational inferences (Pohl et al. 2005). While the correlation length of the magnetic field increases with time, it is at all times less than the size of the box by a factor of several.

On the other hand, increasing the shock velocity from  $10^{-2}c$  to near  $c$  would raise  $\mathcal{J}$  by a factor of  $10^6$ , thereby speeding up the rate of field amplification by  $\mathcal{J}^{6\delta} \geq 10^3$  while decreasing the expansion time by only a factor of  $10^2$ , so there would then seem to be enough time to amplify the magnetic field by many orders of magnitude even on the largest scale—as demonstrated in our simulations—if there are no other fundamental limitations that we have not yet identified. Thus, GRBs, which create ultrarelativistic shocks in the interstellar medium, would have the greatest potential for magnetic field amplification, because their ratio of particle pressure to initial magnetic pressure is so large. This is now discussed below.

In our simulations, the velocity of the turbulence attains a magnitude of about  $10^2 v_{A0}$ , the magnetic field increases to  $\sim 10$  times the original field  $B_0$ , and the correlation length  $L$  of this field is about  $10^{-1}$  of the box size  $R$ . Thus, the quantity  $eBL$  is not much changed from the original value  $eB_0 R$ , meaning that the maximum energy attainable by CRs,  $\sim u_s eBL/c$  (Eichler & Pohl 2011), is not much changed by the magnetic field amplification. (However, until we are certain how the final correlation length scales with the running time of the simulation, this matter remains not completely settled.)

If the energy of the highest energy CRs  $E$  is taken to be  $u_s B_0 R/c$  then the deflection of these highest energy CRs implied by, though ignored in, the simulations is probably small for  $u_{\text{rms}} \ll u_s$ . In general, the turbulent rms velocity  $u_{\text{rms}}$  should be somewhat less than the shock velocity,  $u_s$ , so the potential drop  $e u_{\text{rms}} BL/c$  across one correlation length  $L$  is somewhat less than the maximum energy attainable with shock acceleration  $e u_s BL/c$ . This means that deflection is not a problem for the highest energy CRs but would be a problem for lower energy CRs, and, to compute the CR current, we are entitled to figure in only CRs of the highest energies, i.e., above  $u_{\text{rms}} E_{\text{max}}/u_s$ . Magnetic field amplification that uses CRs at lower energies is unlikely to help increase the maximum energy to which CRs can be accelerated by shocks.

As mentioned above, the correlation length  $L$  is probably considerably less than the size of the box, i.e., the radius of the SNR when applied to that context. It is possible that the rather large values of magnetic fields that have been claimed for young SNRs ( $10^3 G$ , i.e., about  $10^2$  times the interstellar field of the Galaxy) are observationally compatible with such a small scale.

### 5.2. Weakly Magnetized Relativistic Shock Waves

We define a weakly magnetized relativistic shock wave as one where the kinetic energy of the upstream fluid flowing into the shock greatly exceeds the magnetic energy, i.e., where the upstream fluid is sufficiently magnetized as to be describable by MHD. Particles reflecting off the shock have velocity  $\beta_s$  in the frame of the shock, where  $u_s = \beta_s c$  is the shock velocity, which we assume to be equal to the streaming velocity discussed in Section 1. Assuming  $(1 - \beta_s) \ll 1$ , velocities are up to  $\beta_s + (1 - \beta_s)/2$  in the lab frame. The thickness of the shock precursor in the lab frame is thus of order  $R_s(1 - \beta_s)/2$ , where  $R_s$  is the radius of the shock. The current density in reflected ions, which we assume extend farther upstream than the reflected electrons, is thus of order

$$J \simeq 2en_0c\Gamma_s^2. \quad (42)$$

For typical GRB parameters  $n_0 \sim 1\text{cm}^{-3}$ ,  $u_s \simeq c$ ,  $\Gamma_{s2} \equiv \Gamma_s/100$  (where  $\Gamma_s$  is the shock Lorentz factor), and  $B_0 \sim 3\mu G$ , the dimensionless parameter defined in the introduction is  $\mathcal{J} \sim n_0 m_i c^2 / (B_0^2 / 8\pi) = \Gamma_s^2 c^2 / v_A^2 \sim 10^{13} \Gamma_{s2}^2$  for scales  $k^{-1}$  of order the reflected ion gyroradius. This is a far larger value than anything that can be reliably simulated, because the fastest growing mode is of too small a scale to be resolvable numerically.

The thickness of the precursor of reflected ions from the shock is determined by how far ahead of the shock the ions can get before they are overtaken by the shock. A reflected ion by definition moves faster along the shock normal than the shock itself at the moment the ion crosses upstream, and it is overtaken by the shock after it has gyrated approximately  $1/\Gamma_s$  of its gyroradius  $r_g \simeq \Gamma_s^2 m_i c^2 / eB_0$ , at which point its motion along the shock normal is less than that of the shock, so the shock overtakes it. Thus, it has moved a distance of  $\Delta r = r_g / \Gamma_s = \Gamma_s m_i c^2 / eB_0$ , whereas the shock has moved by  $\beta_s \Delta r$ . The thickness of the precursor is then  $(1 - \beta_s)\Delta r \simeq m_i c^2 / \Gamma_s eB_0$ .

The time over which a parcel of fluid at radius  $R$  is exposed to the reflected ion flux is

$$\Delta t = \Delta r(1 - \beta_s)/c, \quad (43)$$

and its ratio to the Alfvén crossing time across the precursor is

$$\frac{\Delta t}{R/v_A} = v_A/c. \quad (44)$$

Due to numerical limitations, it remains unclear how much magnetic field amplification can take place. While we have shown that perturbations can grow by many orders of magnitude, we do not have any runs in which the final magnetic field was more than a factor of 10 or so more than the original field. As we do not understand the nonlinear dissipation of magnetic field, so we do not know a priori how the limiting field scales with  $\mathcal{J}$ . Yet we argue on theoretical grounds that the  $\alpha^2$ -dynamo should be able to amplify the field at relativistic or near-relativistic

shocks by a large factor, as it apparently does in many compact objects, and the existence of such a dynamo is ultimately due to the left–right asymmetry of the magnetic turbulence that is generated by the CRs.

### 5.3. Cosmic Rays in the Galaxy

Let us now consider systems with lifetimes that are large compared to the Alfvén crossing time, such as the Galaxy. Here, there is enough time for the standard  $\alpha\Omega$  mean-field dynamo to work if there is a source of right–left asymmetric turbulence (Ruzmaikin et al. 1988; Brandenburg & Subramanian 2005). In any system where the magnetic energy has attained rough equipartition between magnetic field and CR pressure, the ratio on the right-hand side of Equation (1) obeys  $8\pi P^{\text{cr}}/B^2 \lesssim 1$ . The first ratio on the right-hand side of Equation (1),  $u_s/c$ , must also be less than unity. The third ratio in Equation (1) must also be less than unity for the assumption for the Bell instability (small deflection of the current-bearing CRs) to be valid. It follows that for the above assumptions, the left-hand side  $\mathcal{J} = 4\pi J^{\text{cr}}/ck_1 B_0 \ll 1$ . This, however, means that the Bell instability does not occur, as seen from Equation (9); rather, the effect of the CRs is to slightly decrease the phase velocity of stable Alfvén waves. It follows that Bell turbulence cannot amplify the magnetic field to near equipartition with the CR pressure. Some estimates in the literature use a CR density of  $\sim 10^9\text{cm}^{-3}$ . It would follow that  $\mathcal{J} \gg 1$ . However, the problem here is that this value for the CR density includes low-energy (GeV) CRs, which satisfy the assumption for small deflection only at extremely small spatial scales. It is doubtful that such modes should even be Bell-unstable at all because of the  $-\eta k^2$  damping term in the imaginary part of the frequency, as expressed by Equation (9), which grows with  $k$  faster than the growth term, and which should therefore dominate at small spatial scales.

As discussed in the introduction, the factor  $3P^{\text{cr}}/(B^2/4\pi)$  is of the order of unity for the Galaxy as a whole if all relativistic CRs are included. The anisotropy  $u_s/c$  is bounded by observations to be at most  $10^{-3}$ . Finally, the term  $eB/k\Gamma m_i c^2$  must be less than unity to satisfy the small CR deflection criterion that is the basis for the Bell instability. Altogether it follows that the quantity  $\mathcal{J}$  in Equation (1) is less than unity in the Galactic disk. This, however, implies Bell stability by Equation (9). So, whereas the standard  $\alpha\Omega$  mean-field dynamo (Ruzmaikin et al. 1988; Brandenburg & Subramanian 2005) and tangling the Galactic magnetic field with CR streaming instabilities may be viable ways to amplify the Galactic magnetic field, resonant CR streaming instabilities seem the more promising way to do it over large volumes, where  $3P^{\text{cr}}/(B^2/4\pi)$  is of the order of unity. Resonant CR streaming instabilities produce Alfvén modes of preferential circular polarization, just as the Bell instability does, so the theoretical mechanisms for field amplification that are discussed in this paper apply to them as well.

We conclude that dynamo activity in the Galactic disk from the twisting of the field by collective CR interactions can take place in principle. The numbers seem marginal, so more careful investigation is needed to settle this point.

### 5.4. Unconfined Intergalactic Cosmic Rays

In intergalactic space, the CR pressure is comparable to the magnetic pressure and there is then the chance that  $\mathcal{J}$  greatly exceeds unity. Assuming that streaming instabilities keep the streaming velocity below the Alfvén velocity  $v_A$ , we can replace

$u_s$  with  $v_A$ , so in principle the field can be amplified to the point where the magnetic pressure  $B^2/4\pi$  is of the order of  $P^{\text{cr}}v_A/c$ .

We use the following parameters for plasma and CR particles: we assume  $u^{\text{cr}} = 3 \times (10^6\text{--}10^7)\text{ cm s}^{-1}$  for the drift velocity of CR particles,  $n^{\text{cr}} = 10^{-9}$  to  $10^{-10}\text{ cm}^{-3}$  for the number density of CR particles,  $n_i = 10^{-4}$  to  $10^{-2}\text{ cm}^{-3}$  for the mean number density of plasma ions,  $B_* = 1\text{ }\mu\text{G}$  for the equilibrium mean magnetic field, and  $\ell_0 = 3 \times 10^{18}\text{ cm}$  for the turbulent length scale. The Alfvén speed is  $v_A = 10^8\text{--}10^9\text{ cm s}^{-1}$ , and the dimensionless  $\mathcal{J}$  parameter is

$$\frac{4\pi}{c} \frac{J^{\text{cr}}\ell_0}{B_*} \approx 10^2\text{--}10^5, \quad (45)$$

which is comparable to the values studied in this paper.

## 6. CONCLUSIONS

We have investigated the mean-field dynamo mechanisms in a turbulent plasma with a CR current. We find a linear growth stage, corresponding to the Bell instability, and then a nonlinear stage corresponding to the production of a fully developed MHD turbulence and generation of larger-scale magnetic field.

In the nonlinear stage, the level of MHD turbulence continues to grow (see Figures 2 and 4), and the correlation length increases with time (see Figure 9). The turbulence develops an  $E_M(k) \propto k^{-5/3}$  spectrum, despite the fact that the initial spectrum is  $E_M(k) \propto k^4$ . These effects were far from obvious, even given the stirring by the counter- $J^{\text{cr}} \times B$  forces on the fluid, which is the basis of the Bell instability.

We suggest that this combination of magnetic field amplification and large-scale ordering is due to the  $\alpha^2$  dynamo instability, in which the original field is stretched by unstable Alfvén modes, and then the stretched component is itself stretched by unstable circularly polarized Alfvén modes. This effect is to be contrasted with the long-wavelength linear instability discussed by Bykov et al. (2011), because their growth rate vanishes when the perturbations are independent of  $z$ . According to the simulations, the level of magnetic field on any scale can be enhanced by a factor of several within one expansion time, even at the largest scales, but there is no direct numerical evidence at present that it can be enhanced by much more than that. Nevertheless, the analysis presented here predicts that much larger enhancement, via exponential growth to the  $\alpha$  effect, is possible.

We have also used DNS and the test-field method to confirm our analysis. DNS shows that the instability has three stages. In the first stage, the Bell instability is excited; in the intermediate stage the linear growth continues among the high- $k$  modes, while mode coupling feeds the low- $k$ , large-scale modes. In the third stage, growth on large scale continues, apparently due to the  $\alpha^2$  dynamo.

We find, as expected, that the value of  $\alpha$ , which has units of velocity, can never be much greater than the rms turbulent velocity,  $u_{\text{rms}}$ . The rms turbulent velocity,  $u_{\text{rms}}$ , by energy conservation must be less than the shock velocity  $u_s$ , probably much less. Thus, the maximum scale to which the  $\alpha^2$  dynamo can operate efficiently must be limited to  $\alpha/u_s \ll 1$  of the radius of the blast wave  $R$ ; because  $\alpha \lesssim u_{\text{rms}} \ll u_s$ , there is not enough time in a single expansion time to stretch or move the field significantly over the characteristic expansion time  $R/u_s$  of the blast wave. There is enough time only to greatly amplify the field on scales much smaller than  $R$ . Similar remarks would apply to accretion shocks, since material is swept out of the region of field amplification over a timescale of  $R/u_s$ .

In blast waves from GRBs, on the other hand, this maximum scale of amplification,  $\alpha\Delta/c$  (where  $\Delta$  is the scale of the CR precursor), could be much larger than the ion skin depth, so dynamo activity in the precursors of such blast waves could significantly increase the magnetic correlation length relative to what is produced by the Weibel instability, so that the ohmic dissipation downstream would not be so devastating.

The maximum energy to which CRs can be accelerated by expanding SNRs, which is proportional to  $B_0R$  without magnetic field amplification, is not greatly enhanced by large-scale field amplification (not, at least, in the parameter regime we have explored), since the increase in field strength comes at the cost of decreased correlation length  $L$ , and the product  $BL$  is enhanced far less than  $B$ . However, quantification of this point, made in greater detail by Eichler & Pohl (2011), would require a more extensive library of simulations, for all values of the ion current parameter  $\mathcal{J}$  that could conceivably occur in nature, and such simulations become very difficult for high  $\mathcal{J}$ . Clearly if the pressure of initial field is sufficiently small relative to the CR pressure, then extremely large values of  $\mathcal{J}$  are possible, and the range  $\mathcal{J} \gg 10^3$  has not been explored numerically. On the basis of extrapolation of the two values of  $\mathcal{J}$  ( $\mathcal{J} = 80$  or  $800$ ) for which we run high-resolution simulations, the  $e$ -folding timescale for field amplification  $t(\mathcal{J}, k)$  over scale  $\pi k^{-1}$  is approximately  $C[v_A k \mathcal{J}^\delta]^{-1}$  ( $C \sim 1, \delta \sim 0.7$ ), while we expect on the basis of Equation (1) that the largest allowable value of  $\mathcal{J}$ , which occurs at  $eB/[k\Gamma m_i c^2] \sim 1$ , scales as  $v_A^{-2}$ . So the timescale for field amplification scales as  $v_A^{-1+2\delta} k^{-1} \sim v_A^{0.4} k^{-1} \propto B_0^{0.4} k^{-1}$ . Clearly this timescale can be made small enough for sufficiently weak fields and sufficiently small spatial scales (i.e., high  $k$ ). How field amplification at these scales and field strengths would ultimately affect the capability of shock acceleration remains an important question for future research.

We have also considered the potential of this dynamo process in steady situations where newly created magnetic flux does not quickly sweep through the region where CRs stream. An example of this could be the Galaxy itself, with escaping CR providing a steady flux over the lifetime of the Galaxy. If we assume that the CRs that provide current for growth on scale  $k^{-1}$  must satisfy  $eB/[k\Gamma m_i c^2] \leq 1$ , then, by Equation (1), the condition that  $\mathcal{J} \geq 1$  requires that  $P^{\text{cr}} \gg (B^2/8\pi)(c/u_s)$  (where  $u_s$  now stands for CR streaming velocity), so the dynamo can only bring the magnetic pressure to within a fraction  $u_s/c$  of the CR pressure. On the other hand, this may be interesting, because it could “sprout” a seed magnetic field to a sufficiently large amplitude that some other mechanism, such as the magnetorotational instability, could further raise the field pressure to its present value,  $\sim P^{\text{cr}}$ .

We have also noted that resonant CR streaming instability, coupled with differential rotation, remains a possible way to promote an  $\alpha\Omega$  dynamo in the Galactic disk.

We thank Yuri Lyubarsky for helpful discussions. We acknowledge the NORDITA dynamo program of 2011 for providing a stimulating scientific atmosphere. This work was supported in part by the Swedish Research Council Grant No. 621-2007-4064, the European Research Council under the AstroDyn Research Project 227952 (A.B.), and by the Israel Science Foundation governed by the Israeli Academy of Sciences, the Israel-U.S. Binational Science Foundation, and the Joan and Robert Arnow Chair of Theoretical Astrophysics (D.E.). The authors (I.R. and N.K.) acknowledge the hospitality of NORDITA.

## APPENDIX

DERIVATION OF EQUATION FOR TOTAL  $\alpha$  EFFECT

We determine the contributions to the mean EMF,  $\mathcal{E}(\overline{\mathbf{B}}) = \overline{\mathbf{u} \times \mathbf{b}}$ , caused by CR particles in homogeneous turbulent plasma. The procedure of the derivation of equation for the mean EMF is as follows. We use a mean-field approach in which the magnetic and velocity fields are divided into the mean and fluctuating parts, where the fluctuating parts have zero mean values. The momentum and induction equations for the turbulent fields are given by

$$\overline{\rho} \frac{\partial \mathbf{u}(t, \mathbf{x})}{\partial t} = -\nabla p_{\text{tot}} + \frac{1}{4\pi} [(\mathbf{b} \cdot \nabla) \overline{\mathbf{B}} + (\overline{\mathbf{B}} \cdot \nabla) \mathbf{b}] - \frac{1}{c} \overline{\mathbf{J}^{\text{cr}}} \times \mathbf{b} + \frac{1}{c} \text{en}^{\text{cr}} (\mathbf{u} \times \overline{\mathbf{B}}) + N^u, \quad (\text{A1})$$

$$\frac{\partial \overline{\mathbf{b}}(t, \mathbf{x})}{\partial t} = (\overline{\mathbf{B}} \cdot \nabla) \mathbf{u} - (\mathbf{u} \cdot \nabla) \overline{\mathbf{B}} - \overline{\mathbf{B}} (\nabla \cdot \mathbf{u}) + N^b, \quad (\text{A2})$$

where  $\mathbf{u}$  and  $\mathbf{b}$  are fluctuations of velocity and magnetic field,  $\overline{\mathbf{B}}$  is the mean magnetic field,  $\overline{\mathbf{J}^{\text{cr}}}$  is the mean density of the electric current of CR particles,  $N^u$  and  $N^b$  are the nonlinear terms which include the molecular dissipative terms,  $p_{\text{tot}} = p + (\overline{\mathbf{B}} \cdot \mathbf{b})/4\pi$  are the fluctuations of total pressure, and  $p$  are the fluctuations of fluid pressure. To exclude the pressure term from the equation of motion (A1), we calculate  $\nabla \times (\nabla \times \mathbf{u})$ . Then we rewrite the obtained equation and Equation (A2) in Fourier space.

## A.1. Two-scale Approach

We apply the two-scale approach, e.g., a correlation function,

$$\begin{aligned} \overline{u_i(\mathbf{x})u_j(\mathbf{y})} &= \int d\mathbf{k}_1 d\mathbf{k}_2 \overline{u_i(\mathbf{k}_1)u_j(\mathbf{k}_2)} \exp\{i(\mathbf{k}_1 \cdot \mathbf{x} + \mathbf{k}_2 \cdot \mathbf{y})\} \\ &= \int d\mathbf{k} d\mathbf{K} f_{ij}(\mathbf{k}, \mathbf{K}) \exp(i\mathbf{k} \cdot \mathbf{r} + i\mathbf{K} \cdot \mathbf{R}) \\ &= \int d\mathbf{k} f_{ij}(\mathbf{k}, \mathbf{R}) \exp(i\mathbf{k} \cdot \mathbf{r}) \end{aligned}$$

(see, e.g., Roberts & Soward 1975). Hereafter, we omitted argument  $t$  in the correlation functions,  $f_{ij}(\mathbf{k}, \mathbf{R}) = \hat{L}(u_i; u_j)$ , where

$$\hat{L}(a; c) = \int \overline{a(\mathbf{k} + \mathbf{K}/2)c(-\mathbf{k} + \mathbf{K}/2)} \exp(i\mathbf{k} \cdot \mathbf{R}) d\mathbf{K},$$

and we introduced new variables  $\mathbf{R} = (\mathbf{x} + \mathbf{y})/2$ ,  $\mathbf{r} = \mathbf{x} - \mathbf{y}$ ,  $\mathbf{K} = \mathbf{k}_1 + \mathbf{k}_2$ ,  $\mathbf{k} = (\mathbf{k}_1 - \mathbf{k}_2)/2$ . The variables  $\mathbf{R}$  and  $\mathbf{K}$  correspond to the large scales, while  $\mathbf{r}$  and  $\mathbf{k}$  correspond to the small scales. This implies that we assumed that there exists a separation of scales, i.e., the maximum scale of turbulent motions  $\ell_0$  is much smaller than the characteristic scale  $L_B$  of inhomogeneity of the mean magnetic field.

## A.2. Equations for the Second Moments

We derive equations for the following correlation functions:  $f_{ij}(\mathbf{k}, \mathbf{R}) = \hat{L}(u_i; u_j)$ ,  $h_{ij}(\mathbf{k}, \mathbf{R}) = (4\pi \overline{\rho})^{-1} \hat{L}(b_i; b_j)$ , and  $g_{ij}(\mathbf{k}, \mathbf{R}) = \hat{L}(b_i; u_j)$ . The equations for these correlation functions are given by

$$\begin{aligned} \frac{\partial f_{ij}(\mathbf{k})}{\partial t} &= i(\mathbf{k} \cdot \overline{\mathbf{B}}) \Phi_{ij} + D_{im}(\mathbf{k}_1) f_{mj} + D_{jm}(\mathbf{k}_2) f_{im} \\ &\quad + A_{im}(\mathbf{k}_1) g_{mj}(\mathbf{k}) + A_{jm}(\mathbf{k}_2) g_{im}(-\mathbf{k}) + I_{ij}^f + f_{ij}^N, \end{aligned} \quad (\text{A3})$$

$$\begin{aligned} \frac{\partial h_{ij}(\mathbf{k})}{\partial t} &= -i(\mathbf{k} \cdot \overline{\mathbf{B}}) \Phi_{ij} + ik_n [g_{in}(\mathbf{k}) \overline{B}_j \\ &\quad - g_{jn}(\mathbf{k}) \overline{B}_i] + I_{ij}^h + h_{ij}^N, \end{aligned} \quad (\text{A4})$$

$$\begin{aligned} \frac{\partial g_{ij}(\mathbf{k})}{\partial t} &= i(\mathbf{k} \cdot \overline{\mathbf{B}}) [f_{ij}(\mathbf{k}) - h_{ij}(\mathbf{k}) - h_{ij}^{(H)}] - ik_m \overline{B}_i f_{mj} \\ &\quad + D_{jm}(\mathbf{k}_2) g_{im}(\mathbf{k}) + (4\pi \overline{\rho}) A_{jm}(\mathbf{k}_2) h_{im} + I_{ij}^g + g_{ij}^N, \end{aligned} \quad (\text{A5})$$

where  $\Phi_{ij}(\mathbf{k}) = (4\pi \overline{\rho})^{-1} [g_{ij}(\mathbf{k}) - g_{ji}(-\mathbf{k})]$ . Hereafter, we omitted argument  $\mathbf{R}$  in the correlation functions and neglected terms  $\sim O(\nabla_{\mathbf{R}}^2)$ ,

$$\begin{aligned} D_{ij} &= 2\varepsilon_{ijp} \tilde{\Omega}_q^{\text{cr}} k_{pq}, \quad A_{ij} = 2\varepsilon_{ijp} J_q^{\text{cr}} k_{pq}, \\ \tilde{\Omega}^{\text{cr}} &= \frac{\text{en}^{\text{cr}} \overline{\mathbf{B}}}{2c \overline{\rho}}, \quad \mathbf{J}^{\text{cr}} = \frac{\overline{\mathbf{J}^{\text{cr}}}}{2c \overline{\rho}}, \end{aligned} \quad (\text{A6})$$

$\varepsilon_{ijm}$  is the fully antisymmetric Levi-Civita tensor; the terms  $f_{ij}^N$ ,  $h_{ij}^N$ , and  $g_{ij}^N$  are determined by the third moments appearing due to the nonlinear terms; the source terms  $I_{ij}^f$ ,  $I_{ij}^h$ , and  $I_{ij}^g$ , which contain the large-scale spatial derivatives of the mean magnetic and velocity fields, are given by Equations (A3)–(A6) in Rogachevskii & Kleorin (2004). These terms determine turbulent magnetic diffusion and effects of nonuniform mean velocity on mean EMF. In the present study, we neglect small effects of CR particles on the turbulent magnetic diffusion.

For the derivation of Equations (A3)–(A5) we use an approach that is similar to that applied in Rogachevskii & Kleorin (2004). We took into account that the terms with symmetric tensors with respect to the indices  $i$  and  $j$  in Equation (A5) do not contribute to the mean EMF because  $\mathcal{E}_m = \varepsilon_{mji} g_{ij}$ . We split all tensors into non-helical,  $h_{ij}$ , and helical,  $h_{ij}^{(H)}$ , parts. The helical part of the tensor of magnetic fluctuations  $h_{ij}^{(H)}$  depends on the magnetic helicity, and the equation for  $h_{ij}^{(H)}$  follows from the magnetic helicity conservation arguments (see, e.g., Rogachevskii & Kleorin 2004; Brandenburg & Subramanian 2005, and references therein).

A.3.  $\tau$ -approach

The second-moment Equations (A3)–(A5) include the first-order spatial differential operators  $\hat{N}$  applied to the third-order moments  $M^{(\text{III})}$ . A problem arises how to close the system, i.e., how to express the set of the third-order terms  $\hat{N} M^{(\text{III})}$  through the lower moments  $M^{(\text{II})}$ . We use the spectral  $\tau$  approximation, which postulates that the deviations of the third-moment terms,  $\hat{N} M^{(\text{III})}(\mathbf{k})$ , from the contributions to these terms afforded by the background turbulence,  $\hat{N} M^{(\text{III},0)}(\mathbf{k})$ , are expressed through the similar deviations of the second moments:

$$\hat{N} M^{(\text{III})}(\mathbf{k}) - \hat{N} M^{(\text{III},0)}(\mathbf{k}) = -\frac{1}{\tau(k)} [M^{(\text{II})}(\mathbf{k}) - M^{(\text{II},0)}(\mathbf{k})] \quad (\text{A7})$$

(Orszag 1970; Pouquet et al. 1976; Kleorin et al. 1990; Rogachevskii & Kleorin 2004), where  $\tau(k)$  is the scale-dependent relaxation time, which can be identified with the correlation time of the turbulent velocity field. The quantities with the superscript (0) correspond to the background turbulence (see below). We apply the spectral  $\tau$  approximation only for the non-helical part  $h_{ij}$  of the tensor of magnetic fluctuations.

#### A.4. Solution of Equations for the Second Moments

First we solve Equations (A3)–(A5) neglecting the sources  $I_{ij}^f, I_{ij}^h, I_{ij}^g$  with the large-scale spatial derivatives. Then we will take into account the terms with the large-scale spatial derivatives by perturbations. We subtract from Equations (A3)–(A5) the corresponding equations written for the background turbulence, use the spectral  $\tau$  approximation, and neglect the terms with the large-scale spatial derivatives. We assume that the CR velocity is much larger than fluid velocity, so that the terms  $\propto D_{ij}$  in Equations (A3)–(A5) vanish. Next, we neglect the effect related to the compressibility of the turbulent velocity field. Such effects are important when the Mach number is of the order of or larger than 1. We also assume that the characteristic time of variation of the second moments is substantially larger than the correlation time  $\tau(k)$  for all turbulence scales. This allows us to get a stationary solution for the equations for the second-order moments,  $M^{(II)}$ . Thus, we arrive to the following steady-state solution of Equations (A3)–(A5):

$$\hat{f}_{ij}(\mathbf{k}) \approx f_{ij}^{(0)}(\mathbf{k}) + i\tau(\mathbf{k} \cdot \bar{\mathbf{B}})\hat{\Phi}_{ij}(\mathbf{k}) + \tau [A_{im} \hat{g}_{mj}(\mathbf{k}) + A_{jm} \hat{g}_{im}(-\mathbf{k})], \quad (\text{A8})$$

$$\hat{h}_{ij}(\mathbf{k}) \approx h_{ij}^{(0)}(\mathbf{k}) - i\tau(\mathbf{k} \cdot \bar{\mathbf{B}})\hat{\Phi}_{ij}(\mathbf{k}), \quad (\text{A9})$$

$$\hat{g}_{ij}(\mathbf{k}) \approx g_{ij}^{(0)}(\mathbf{k}) + i\tau(\mathbf{k} \cdot \bar{\mathbf{B}})[\hat{f}_{ij}(\mathbf{k}) - \hat{h}_{ij}(\mathbf{k})] + \tau(4\pi\bar{\rho})A_{jm} \hat{h}_{im}(\mathbf{k}), \quad (\text{A10})$$

where  $\hat{f}_{ij}, \hat{h}_{ij}$ , and  $\hat{g}_{ij}$  are solutions without the sources  $I_{ij}^f, I_{ij}^h$ , and  $I_{ij}^g$ . In the present study we consider linear effects in perturbations of the mean magnetic field. The nonlinear mean-field modeling in turbulent compressible MHD flows with CRs is a subject of a separate ongoing study.

#### A.5. Model for the Background Turbulence

Now we need a model for the background anisotropic turbulence (see Equations (A8)–(A10)). The anisotropy is caused by the equilibrium mean magnetic field  $\bar{\mathbf{B}}_*$ . Generally, a model of an anisotropic turbulence with one preferential direction can be constructed as a combination of three-dimensional isotropic turbulence and two-dimensional turbulence in the plane perpendicular to the preferential direction (see, e.g., Elperin et al. 2002). Also we take into account that the tensor  $f_{ij}^{(0)}(\mathbf{k})$  is the sum of non-helical and helical parts of the turbulence. A non-zero kinetic helicity is caused by the Bell instability. To relate the velocity fluctuations' tensor  $f_{ij}^{(0)}(\mathbf{k})$  with the magnetic fluctuations' tensor  $h_{ij}^{(0)}(\mathbf{k})$  and the cross-helicity tensor  $g_{ij}^{(0)}(\mathbf{k})$ , we use the relation between the magnetic and the velocity fields in the Bell mode:  $\mathbf{b}^{(0)}(\mathbf{k}) = i(\mathbf{k} \cdot \mathbf{B}_*)\mathbf{u}^{(0)}(\mathbf{k})/\gamma_B$ , where  $\gamma_B$  is determined by Equation (9). We use the following model for the background anisotropic homogeneous and helical turbulence caused by the Bell instability:

$$f_{ij}^{(0)}(\mathbf{k}) \equiv \overline{u_i^{(0)}(\mathbf{k})u_j^{(0)}(-\mathbf{k})} = \frac{E(k)}{8\pi k^2} \left\{ [(1-\epsilon)(\delta_{ij} - k_{ij}) + 2\epsilon(\delta_{ij} - e_i e_j - k_{ij}^\perp)] \times \overline{[\mathbf{u}^{(0)}]^2} - \frac{i}{k^2} \varepsilon_{ijn} k_n \overline{\mathbf{u}^{(0)} \cdot (\nabla \times \mathbf{u}^{(0)})} \right\}, \quad (\text{A11})$$

$$h_{ij}^{(0)}(\mathbf{k}) \equiv \frac{\overline{b_i^{(0)}(\mathbf{k})b_j^{(0)}(-\mathbf{k})}}{4\pi\bar{\rho}} = (L^{\text{cr}} k) f_{ij}^{(0)}(\mathbf{k}), \quad (\text{A12})$$

$$g_{ij}^{(0)}(\mathbf{k}) \equiv \overline{b_i^{(0)}(\mathbf{k})u_j^{(0)}(-\mathbf{k})} = (4\pi\bar{\rho} L^{\text{cr}} k)^{1/2} \frac{i(\mathbf{k} \cdot \bar{\mathbf{B}}_*)}{|\mathbf{k} \cdot \bar{\mathbf{B}}_*|} f_{ij}^{(0)}(\mathbf{k}), \quad (\text{A13})$$

where  $L^{\text{cr}} = c\bar{B}_*/(4\pi J^{\text{cr}})$ ,  $E(k) = (q-1)\ell_0(\ell_0 k)^{-q}$  is the energy spectrum function, the length  $\ell_0$  is the maximum scale of turbulent motions,  $\mathbf{e}$  is the unit vector directed along the equilibrium mean magnetic field  $\bar{\mathbf{B}}_*$ ,  $\delta_{ij}$  is the Kronecker unit tensor,  $0 < \epsilon \leq 1$  is the anisotropy parameter of turbulence,  $\mathbf{k} = \mathbf{k}^\perp + k_z \mathbf{e}$ ,  $k_z = (\mathbf{k} \cdot \mathbf{e})$ ,  $k_{ij} = k_i k_j / k^2$ , and  $k_{ij}^\perp = k_i^\perp k_j^\perp / (\mathbf{k}^\perp)^2$ . The turbulent correlation time is  $\tau(k) = C_\tau \tau_0 (\ell_0 k)^{-\mu}$ , where the time  $\tau_0 = \ell_0 / u_0$ ,  $u_0 = \sqrt{[\mathbf{u}^{(0)}]^2}$  is the characteristic turbulent velocity in the scale  $\ell_0$ , and  $C_\tau$  is the coefficient. For the background turbulence with a constant dissipation rate of turbulent energy in inertial range of scales, the exponent  $\mu = q - 1$ , the energy spectrum  $E(k) \propto -d\tau/dk$ , and the coefficient  $C_\tau = 2$ .

Using the solution of the derived second-moment Equations (A8)–(A10), we determine the contributions to the mean EMF,  $\mathcal{E}_i^{\text{cr}} = \varepsilon_{imn} \int \overline{b_n(\mathbf{k})u_m(-\mathbf{k})} d\mathbf{k}$ , caused by CR particles in homogeneous turbulent plasma.

#### A.6. Derivations of Contributions to the $\alpha$ Effect

We take into account effects that are linear in the perturbations of the mean magnetic field:  $\tilde{\mathbf{B}} = \bar{\mathbf{B}} - \bar{\mathbf{B}}_*$ , i.e., we consider a kinematic mean-field dynamo. Substituting Equations (A8)–(A9) into Equation (A10), we obtain

$$\hat{g}_{ij}(\mathbf{k}) \approx \hat{g}_{ij}^{(I)}(\mathbf{k}) + \hat{g}_{ij}^{(II)}(\mathbf{k}) + \hat{g}_{ij}^{(III)}(\mathbf{k}), \quad (\text{A14})$$

$$\hat{g}_{ij}^{(I)}(\mathbf{k}) \approx i\tau(\mathbf{k} \cdot \tilde{\mathbf{B}})[\hat{f}_{ij}^{(0)}(\mathbf{k}) - \hat{h}_{ij}^{(0)}(\mathbf{k})], \quad (\text{A15})$$

$$\begin{aligned} \hat{g}_{ij}^{(II)}(\mathbf{k}) &\approx i\tau^2(\mathbf{k} \cdot \tilde{\mathbf{B}})[A_{im} \hat{g}_{mj}^{(0)}(\mathbf{k}) + A_{jm} \hat{g}_{im}^{(0)}(-\mathbf{k}) \\ &\quad - (4\pi\bar{\rho})A_{jm} \hat{\Phi}_{ij}^{(0)}(\mathbf{k})] \\ &= i\tau^2(\mathbf{k} \cdot \tilde{\mathbf{B}})[A_{im} \hat{g}_{mj}^{(0)}(\mathbf{k}) - 3A_{jm} \hat{g}_{mi}^{(0)}(\mathbf{k})], \end{aligned} \quad (\text{A16})$$

$$\hat{g}_{ij}^{(III)}(\mathbf{k}) \approx g_{ij}^{(0)}(\mathbf{k}) + \tau(4\pi\bar{\rho})A_{jm} h_{ij}^{(0)}(\mathbf{k}), \quad (\text{A17})$$

where we have taken into account that  $\hat{g}_{ij}^{(0)}(\mathbf{k}) = \hat{g}_{ji}^{(0)}(\mathbf{k}) = -\hat{g}_{ij}^{(0)}(-\mathbf{k})$ . The mean EMF is given by  $\mathcal{E}_i^{\text{cr}} = \varepsilon_{imn} \int \hat{g}_{nm}(\mathbf{k}) d\mathbf{k}$ , where the tensor  $\hat{g}_{ij}(\mathbf{k})$  is determined by Equation (A14). There are two contributions to the  $\alpha$  effect caused by

1. non-zero kinetic helicity produced by Bell instability; this contribution is determined by the tensor  $\hat{g}_{ij}^{(I)}(\mathbf{k})$ , where the background turbulence  $\hat{f}_{ij}^{(0)}(\mathbf{k})$  is described by the term  $\propto -(i/k^2)\varepsilon_{ijn} k_n \overline{\mathbf{u}^{(0)} \cdot (\nabla \times \mathbf{u}^{(0)})}$  in Equation (A12); and
2. interaction of the mean CR current with small-scale turbulence; this contribution is determined by the tensor  $\hat{g}_{ij}^{(II)}(\mathbf{k})$ , where the background turbulence  $\hat{f}_{ij}^{(0)}(\mathbf{k})$  is determined by the term  $[(1-\epsilon)(\delta_{ij} - k_{ij}) + 2\epsilon(\delta_{ij} - e_i e_j - k_{ij}^\perp)][\mathbf{u}^{(0)}]^2$  in Equation (A12).

The first contribution to the mean EMF caused by a non-zero kinetic helicity effect in the Bell turbulence is given by

$$\begin{aligned}\mathcal{E}_i^{(I)} &= \varepsilon_{imn} \int \hat{g}_{nm}^{(I)}(\mathbf{k}) d\mathbf{k} \\ &= i \varepsilon_{imn} \int \tau(k) (\mathbf{k} \cdot \tilde{\mathbf{B}}) \hat{f}_{nm}^{(0)}(\mathbf{k}) d\mathbf{k} = \alpha_{ij}^{(I)} \tilde{B}_j, \quad (\text{A18})\end{aligned}$$

where  $\alpha_{ij}^{(I)} = \alpha_1^{\text{cr}} \delta_{ij}$  and  $\alpha_1^{\text{cr}}$  is determined by Equation (27). In the derivation of Equation (A18) we have taken into account that  $L^{\text{cr}} k_1 = \mathcal{J}^{-1} \ll 1$ , which allows us to drop contributions  $\propto \hat{h}_{ij}^{(0)}(\mathbf{k})$  in comparison with that proportional to  $\hat{f}_{ij}^{(0)}(\mathbf{k})$ .

The second contribution to the mean EMF,  $\mathcal{E}_i^{(II)}$ , is caused by the non-helical part of the turbulence:

$$\begin{aligned}\mathcal{E}_i^{(II)} &= \varepsilon_{imn} \int \hat{g}_{nm}^{(II)}(\mathbf{k}) d\mathbf{k} = 4i \varepsilon_{imn} \\ &\times \int \tau^2(k) (\mathbf{k} \cdot \tilde{\mathbf{B}}) A_{mp} g_{np}^{(0)}(\mathbf{k}) d\mathbf{k} = \alpha_{ij}^{(II)} \tilde{B}_j, \quad (\text{A19})\end{aligned}$$

where the tensor  $\alpha_{ij}^{(II)} = \alpha_2^{\text{cr}} (\delta_{ij} + e_i e_j)$  and  $\alpha_2^{\text{cr}}$  is determined by Equation (14). The third contribution to the mean EMF,  $\mathcal{E}_i^{(III)} = \varepsilon_{imn} \int \hat{g}_{nm}^{(III)}(\mathbf{k}) d\mathbf{k}$ , is constant and, therefore, does not affect the large-scale dynamo.

#### A.7. Integrals Used in Section A.6

To integrate over the angles in  $\mathbf{k}$  space, we used the following identities:

$$\begin{aligned}\int k_{ijn} \operatorname{sgn}(k_z) \sin \theta d\theta d\varphi &= \frac{\pi}{2} [P_{in}(\mathbf{e}) e_j + P_{jn}(\mathbf{e}) e_i \\ &+ P_{ij}(\mathbf{e}) e_n + 2e_i e_j e_n], \quad (\text{A20})\end{aligned}$$

$$\int \frac{k_i^\perp k_j k_n}{k^3} \operatorname{sgn}(k_z) \sin \theta d\theta d\varphi = \frac{\pi}{2} [P_{ij}(\mathbf{e}) e_n + P_{in}(\mathbf{e}) e_j], \quad (\text{A21})$$

where  $P_{in}(\mathbf{e}) = \delta_{ij} - e_i e_j$  and  $k_z = k \cos \theta$ .

#### A.8. The Realizability Condition

Let us consider the case when the spectral functions for the kinetic helicity,  $\chi(k)$ , and turbulent kinetic energy,  $u_0^2 E(k)$ , are different, where  $\overline{\mathbf{u}^{(0)} \cdot (\nabla \times \mathbf{u}^{(0)})} = \int \chi(k) dk$  and  $[\overline{\mathbf{u}^{(0)}}]^2 = u_0^2 \int E(k) dk$ . The realizability condition for the kinetic helicity (Moffatt 1978) reads

$$\chi(k) \leq u_0^2 E(k) k. \quad (\text{A22})$$

Let us determine the explicit expression for the function  $\chi(k)$  using Equation (26) for the estimate for the kinetic helicity  $\overline{\mathbf{u}^{(0)} \cdot (\nabla \times \mathbf{u}^{(0)})}$  for the Bell background turbulence:

$$\begin{aligned}\overline{\mathbf{u}^{(0)} \cdot (\nabla \times \mathbf{u}^{(0)})} &\propto \frac{\tau \overline{J_j^{\text{cr}}}}{c \bar{\rho}} \overline{u_n^{(0)} \nabla_j b_n^{(0)}} = \left( \frac{4\pi \overline{J^{\text{cr}}} \ell_0}{c \overline{B_*}} \right)^{1/2} \\ &\times \overline{V_A} \frac{u_0^2}{2\ell_0^2} \int (\ell_0 k)^{3/2} \tau(k) E(k) dk, \quad (\text{A23})\end{aligned}$$

where  $E(k) = (q-1) \ell_0 (\ell_0 k)^{-q}$  and  $\tau(k) = 2 \tau_0 (\ell_0 k)^{1-q}$ . Therefore, the function  $\chi(k)$  is given by

$$\chi(k) = \sqrt{\mathcal{J}} \overline{V_A} \frac{u_0}{\ell_0} (\ell_0 k)^{5/2-q} E(k), \quad (\text{A24})$$

and the realizability condition for the kinetic helicity yields

$$\sqrt{\mathcal{J}} \frac{\overline{V_A}}{u_0} \leq (\ell_0 k)^{q-3/2}, \quad (\text{A25})$$

where

$$\mathcal{J} = \frac{4\pi \overline{J^{\text{cr}}} \ell_0}{c \overline{B_*}}, \quad (\text{A26})$$

and the Kolmogorov spectrum corresponds to  $q = 5/3$ .

## REFERENCES

- Amato, E., & Blasi, P. 2009, *MNRAS*, **392**, 1591  
 Bell, A. R. 2004, *MNRAS*, **353**, 550  
 Bell, A. R. 2005, *MNRAS*, **358**, 181  
 Blandford, R., & Eichler, D. 1987, *Phys. Rep.*, **154**, 1  
 Brandenburg, A., & Dobler, W. 2002, *Comp. Phys. Comm.*, **147**, 471  
 Brandenburg, A., Rädler, K.-H., Rheinhardt, M., & Subramanian, K. 2008, *ApJ*, **687**, L49  
 Brandenburg, A., & Subramanian, K. 2005, *Phys. Rep.*, **417**, 1  
 Bykov, A. M., Ellison, D. C., & Renaud, M. 2012, *Space Sci. Rev.*, **166**, 71  
 Bykov, A. M., Osipov, S. M., & Ellison, D. C. 2011, *MNRAS*, **410**, 39  
 Chen, F. F. 2010, *Introduction to Plasma Physics and Controlled Fusion* (New York: Springer)  
 Eichler, D., & Pohl, M. 2011, *ApJ*, **738**, L21  
 Ellison, D. C., & Eichler, D. 1985, *Phys. Rev. Lett.*, **55**, 2735  
 Elperin, T., Kleeorin, N., Rogachevskii, I., & Zilitinkevich, S. S. 2002, *Phys. Rev. E*, **66**, 066305  
 Kleeorin, N. I., Rogachevskii, I. V., & Ruzmaikin, A. A. 1990, *Sov. Phys.—JETP*, **70**, 878  
 Krause, F., & Rädler, K.-H. 1980, *Mean-field Magnetohydrodynamics and Dynamo Theory* (Oxford: Pergamon)  
 Lagage, P. O., & Cesarsky, C. J. 1983, *A&A*, **125**, 249  
 Lucek, S. G., & Bell, A. R. 2000, *Ap&SS*, **272**, 255  
 Luo, Q., & Melrose, D. 2009, *MNRAS*, **397**, 1402  
 Medvedev, M. V., & Loeb, A. 1999, *ApJ*, **526**, 697  
 Moffatt, H. K. 1978, *Magnetic Field Generation in Electrically Conducting Fluids* (Cambridge: Cambridge Univ. Press)  
 Orszag, S. A. 1970, *J. Fluid Mech.*, **41**, 363  
 Parker, E. N. 1979, *Cosmical Magnetic Fields* (New York: Oxford Univ. Press)  
 Pelletier, G., Lemoine, M., & Marcowith, A. 2006, *A&A*, **453**, 181  
 Pohl, M. 2009, *Phys. Rev. D*, **79**, 041301  
 Pohl, M., Yan, H., & Lazarian, A. 2005, *ApJ*, **626**, L101  
 Pouquet, A., Frisch, U., & Léorat, J. 1976, *J. Fluid Mech.*, **77**, 321  
 Reville, B., O’Sullivan, S., Duffy, P., & Kirk, J. G. 2008, *MNRAS*, **386**, 509  
 Rheinhardt, M., & Brandenburg, A. 2010, *A&A*, **520**, A28  
 Riquelme, M. A., & Spitkovsky, A. 2009, *ApJ*, **694**, 642  
 Roberts, P. H., & Soward, A. M. 1975, *Astron. Nachr.*, **296**, 49  
 Rogachevskii, I., & Kleeorin, N. 2004, *Phys. Rev. E*, **70**, 046310  
 Rogachevskii, I., Kleeorin, N., Käpylä, P. J., & Brandenburg, A. 2011, *Phys. Rev. E*, **84**, 056314  
 Ruzmaikin, A., Shukurov, A., & Sokoloff, D. 1988, *Magnetic Fields of Galaxies* (Dordrecht: Kluwer)  
 Schirmer, M., Rädler, K.-H., Schmitt, D., Rheinhardt, M., & Christensen, U. 2005, *Astron. Nachr.*, **326**, 245  
 Schirmer, M., Rädler, K.-H., Schmitt, D., Rheinhardt, M., & Christensen, U. R. 2007, *Geophys. Astrophys. Fluid Dyn.*, **101**, 81  
 Vladimirov, A. E., Bykov, A. M., & Ellison, D. C. 2009, *ApJ*, **703**, L29  
 Zeldovich, Ya. B., Ruzmaikin, A. A., & Sokoloff, D. D. 1983, *Magnetic Fields in Astrophysics* (New York: Gordon and Breach)  
 Zirakashvili, V. N., Ptuskin, V. S., & Völk, H. J. 2008, *ApJ*, **678**, 255  
 Zweibel, E. G., & Everett, J. E. 2010, *ApJ*, **709**, 1412